

CORRELATION LENGTH AND COMPRESSIBILITY FOR
POLAR FLUIDS NEAR THEIR CRITICAL POINTS

A Thesis

Presented to

The Faculty of the Division of Graduate
Studies and Research

by

Edward Matthew Patterson

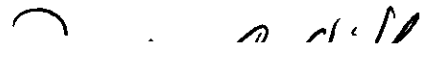
In Partial Fulfillment
of the Requirements for the Degree
Doctor of Philosophy in
The School of Physics

Georgia Institute of Technology

January, 1974

CORRELATION LENGTH AND COMPRESSIBILITY FOR
POLAR FLUIDS NEAR THEIR CRITICAL POINTS

Approved:



Chairman

Date approved by Chairman: 1/22/74

ACKNOWLEDGMENTS

I would like to acknowledge the assistance of Dr. D. C. O'Shea, my thesis advisor, whose timely ideas have been instrumental in the acquisition of data and in its analysis, and whose editorial comments have been very helpful in the actual writing of the thesis. I would also like to thank the members of my reading committee, Dr. H. A. Gersch and Dr. C. S. Kiang, for helpful comments and suggestions. Dr. Kiang has been particularly involved since the inception of the project.

I also thank the Clark College physics department for support during a portion of the thesis research, and in particular, Dr. G. Walker and Dr. D. Stauffer for many helpful discussions. I would also like to thank Dr. H. L. Swinney of the City College of New York for discussions related to the choice of a thesis topic.

Mr. K. B. Springfield, Mr. J. R. Bell, Mr. R. W. Gryder, and Mr. V. Mallette have been very helpful in providing technical assistance. Mrs. Loretta Pharris has typed the final version of the thesis, doing a superb job under less than ideal conditions.

Finally I would like to give a special thanks to my wife, Marjorie, for support and encouragement throughout the thesis project, and for invaluable help in the final preparation of the thesis.

TABLE OF CONTENTS

	Page
ACKNOWLEDGMENTS	ii
LIST OF TABLES	iv
LIST OF ILLUSTRATIONS	v
SUMMARY	vi
CHAPTER	
I. INTRODUCTION	1
II. THEORY OF CRITICAL PHENOMENA	6
Critical Behavior of a Fluid	
Theoretical Models of Critical Behavior	
Universality	
Polar Fluids	
Measurements of Critical Behavior	
Light Scattering Equations for Fluids Near Critical	
Points	
III. EXPERIMENTAL APPARATUS AND PROCEDURES	46
Properties of Sample Fluids	
Sample Preparation	
Temperature Measurement and Control	
Measurements with an Optical Bridge	
IV. DATA AND ANALYSIS	79
Data Analysis Procedure	
Determination of K_T	
Experimental Determination of ξ_0 and ν	
Discussion of Compressibility Results and Comparison	
with Other Experiments	
Conclusions	
APPENDICES	113
BIBLIOGRAPHY	119
VITA	122

LIST OF TABLES

Table	Page
1. Selected Critical Point Exponents	23
2. Selected Exponent Relations from Scaling Laws	29
3. Determination of Sample Cell Volume of the N ₂ O High Pressure Cell	52
4. Calculation of Filling Parameters for N ₂ O Cell	54
5. Calculation of Critical Density for N ₂ O	60
6. Critical Data for N ₂ O, CClF ₃ , and CH ₃ F	61
7. $\kappa_T(\Gamma, \gamma)$, β , α for N ₂ O, CO ₂ , CClF ₃ and CH ₃ F	107

LIST OF ILLUSTRATIONS

Figure	Page
1. Pressure-Temperature Diagram for a Fluid	7
2. Pressure-Density Diagram of a Fluid in the Critical Region	9
3. Van der Waals Isotherms for a Fluid	21
4. Definition of Angles used in Light Scattering Equations	35
5. Exploded View of High Pressure Cell	49
6. Filling System for Sample Cell	56
7. Optical Bridge Components	71
8. Turbidity vs ΔT Data for N_2O	84
9. Effect of Range Variation on N_2O γ	85
10. Turbidity vs ΔT Data for $CClF_3$	90
11. Effect of Range Variation on $CClF_3$ γ	91
12. Turbidity vs ΔT Data for CH_3F	96
13. Effect of Range Variation on CH_3F γ	97
14. Correlation Length vs ΔT Data for N_2O , $CClF_3$, CH_3F . . .	100
15. Effect of Range Variation on ξ for N_2O , $CClF_3$, CH_3F . .	101

SUMMARY

Measurements of the asymptotic behavior of the isothermal compressibility and of the correlation length for polar fluids slightly above their critical points have been made to determine the critical exponents, γ and ν , associated with these quantities for polar fluids and to determine whether the polar nature of these fluids affects the measured values of the critical exponents.

The substances investigated are three polar fluids with a range of polarities, N_2O , very slightly polar, $CClF_3$, with moderate polarity, and CH_3F , with a relatively large polarity. The method used is a light scattering technique in which the turbidity of each fluid is measured as a function of temperature, from which the isothermal compressibility and the correlation length as a function of the temperature difference from the critical temperature may be determined. The critical exponents and coefficients describing the asymptotic behavior of these substances may then be determined by fitting the data to appropriate power laws and varying the range of data for minimum error.

Results show that the exponent describing the asymptotic behavior of the isothermal compressibility for N_2O , γ , is approximately the same as that measured for CO_2 , as expected, since the fluids have similar physical characteristics. The exponent for $CClF_3$ has a slightly lower value with that for CH_3F having a value intermediate between the other two values. Measurements of the exponents describing the asymptotic behavior of the correlation length, ν , show no significant varia-

tion among the three fluids.

There is no variation in the exponents that may be related to the increasing polarity of the fluids, and so the conclusion is that the dipole moments of these fluids do not affect the measured critical exponents. The results, however, are consistent with possible effects on γ due to variations in the shape of the molecules.

CHAPTER I

INTRODUCTION

The study of critical phenomena dates from an 1869 paper by Thomas Andrews¹ who discovered that gases could be condensed to form liquids with an observable phase change only if the gas were below a certain characteristic temperature, different for each gas. He called this characteristic temperature the critical temperature of the gas and described several effects associated with the critical point, notably a large increase in the compressibility and the critical opalescence, the great amount of light scattered from the substance, at the critical point. He also noted that the behavior appeared to be similar for various substances. The behavior observed by Andrews was explained in 1873 by J. D. van der Waals² with his equation of state for gases. This equation, together with some assumptions about the minimization of free energy, described the behavior of gases above the critical temperature as well as that of the two coexisting phases below the critical temperature. The universal nature of critical phenomena was explicitly described by the law of corresponding states which expressed the behavior of a gas solely in terms of ratios of the variables, P , V , T , to their values at the critical point.

Analogous behavior was also found for other systems. Iron was found to lose its ferromagnetic character above a certain temperature. For certain binary mixtures, there was a temperature below which mixing

could not take place. It was soon realized that each of these temperatures was a critical temperature and could be characterized by the same formalism as the gas liquid critical point. Equations describing the behavior resulted in formally similar predictions for each of these diverse systems.

The question of critical opalescence and its relation to the statistical behavior of the fluid system was investigated by von Smoluchowski³ who realized that the critical opalescence was due to light scattered by density fluctuations which become very large at the critical point. Einstein⁴ calculated the magnitude of the scattering in terms of the fluctuations in the thermodynamic variables of the fluid about their average values, but neglected correlations between the fluctuations. These correlations were taken account of by Ornstein and Zernike⁵ who calculated the magnitude of the density fluctuations in terms of the integral of the correlation function for the fluid over the range for which there was correlation in the fluid. They showed that the divergence in the size of the density fluctuations was related to an increase in the correlation length in the fluid and obtained an expression for light scattered by a fluid in the critical region in terms of the correlation length and the compressibility in the fluid.

Detailed studies of the shape of the coexistence curve for fluids and measurements of anomalously large specific heats at the critical points of both fluid and magnetic systems led to the realization that the classical theories (van der Waals and other similar theories) were not quantitatively correct. Correct descriptions were obtained with the Ising model, a model for magnetic systems with only nearest neigh-

bor interactions. The two dimensional Ising model, which predicted non-classical results including logarithmically diverging specific heat at the critical point, was solved by Onsager in 1944. Although the three dimensional Ising model has not been solved exactly, numerical predictions based on this model have proved to give very accurate descriptions of critical behavior. The success of the Ising model in predicting critical behavior is due to the short range nature of its interactions; the incorrect predictions of the classical theories are the result of the fact that each assumes that the behavior of the system is determined by long range forces. At the present time it is thought that the critical behavior is due to very short range forces whose influence propagates indirectly from molecule to molecule resulting in long range correlations. Since the direct interaction is short-ranged the indirect correlations are much more important in determining the behavior of the system than the direct interaction; but the indirect correlations depend on the dimensionality of the system and are influenced only very slightly by the details of the direct interaction. Thus it is expected, and confirmed by experiment, that the critical behavior of systems having the same dimensionality will be the same whether the system is a magnetic or a fluid system; the behavior is expected to be universal.

Close to the critical point, many parameters describing the system converge to zero, or diverge; and thus the asymptotic behavior approaching the critical point may be represented with a power law in temperature difference from the critical temperature. In the early 1960's it was realized that the exponents characterizing these power

laws were of interest in themselves. They provided numerical specifications of critical behavior, and studies of exponent relationships have led to insights into critical behavior and into appropriate forms for the equation of state describing dense fluids. Perhaps the most useful have been the concept of universality and the scaling laws which assume a homogeneous equation of state and derive all exponents for static critical phenomena in terms of two parameters.

Most experimental investigations of critical phenomena are concerned with the determination of the exponents and coefficients describing the asymptotic behavior of systems near their critical points and with verifying exponent relationships. This is often done using traditional pressure-volume-temperature measurement techniques, but such measurements near the critical point are subject to many experimental difficulties. Light scattering and other optical techniques may be used to overcome some of these difficulties.

Measurements of the critical properties of fluid systems have generally supported the ideas of scaling and universality within the limits of experimental accuracy, but nearly all measurements have been made on simple non-polar fluids.

Polar molecules are characterized by a permanent molecular dipole moment, and so there is the possibility of a long range interaction via the dipole moments of the molecules. There is evidence that for certain ferromagnetic and ferroelectric systems, the critical behavior is influenced by the presence of a long range dipole force. Measurements of the coexistence curves of polar molecules show only slight variations from those of non-polar fluids, differences that are probably not signif-

icant; but the one reported measurement⁶ of the compressibility of a polar fluid results in a value for the exponent that is different from that which would be predicted on the basis of universality.

The purpose of this investigation is to determine the asymptotic behavior of the compressibility and the correlation length for several polar fluids, one with a very small dipole moment, one with a moderate dipole moment, and one with a relatively large dipole moment, to determine the exponents that are characteristic of the asymptotic behavior, and to determine whether there is any consistent deviation from the behavior predicted on the basis of universality that may be related to the effects of the increasing strength of the dipole-dipole interaction in these fluids.

The method used in this investigation is a light scattering technique, the measurement of the extinction coefficient, the turbidity, of the fluid as a function of the temperature difference from the critical point. The turbidity is related by Ornstein-Zernike theory to the magnitude of the compressibility and the correlation length in the fluid; and so the temperature dependence of the turbidity may be used to determine the temperature dependence of the compressibility and correlation length, from which the exponents characterizing these quantities may be calculated. The behavior of the fluids may then be analyzed in terms of the exponents and the relation of the measured exponents to those measured for non-polar systems.

CHAPTER II

THEORY OF CRITICAL PHENOMENA

Critical Behavior of a Fluid

A fluid system may be represented by an equation of state relating the pressure, density, and temperature (P , ρ , T) of the system. The general behavior of such a system may be represented graphically by Figures 1 and 2; Figure 1 shows the pressure and temperature values for which the system may exist as a solid, liquid, or gas. Within each phase, gas or liquid for example, changes in the pressure or the temperature are accompanied by continuous changes in the density of the phase. The density is not continuous across the vapor pressure curve. For example, liquid water at 100° C and one atmosphere pressure does not have the same density as water vapor under the same conditions. As the temperature increases the density difference between the liquid and the gas phases across the vapor pressure curve decreases. At the end of the vapor pressure curve, where the densities of the gas and the liquid are equal, there is a critical point characterized by the following parameters: temperature (T_c), pressure (P_c) and density (ρ_c). The critical temperature is that temperature above which the system does not exhibit a discontinuous phase change, while below T_c the system may exist as one or two phases, depending on the conditions of temperature and pressure. The critical density is that density to which the liquid and the gas densities converge at the critical temperature. The

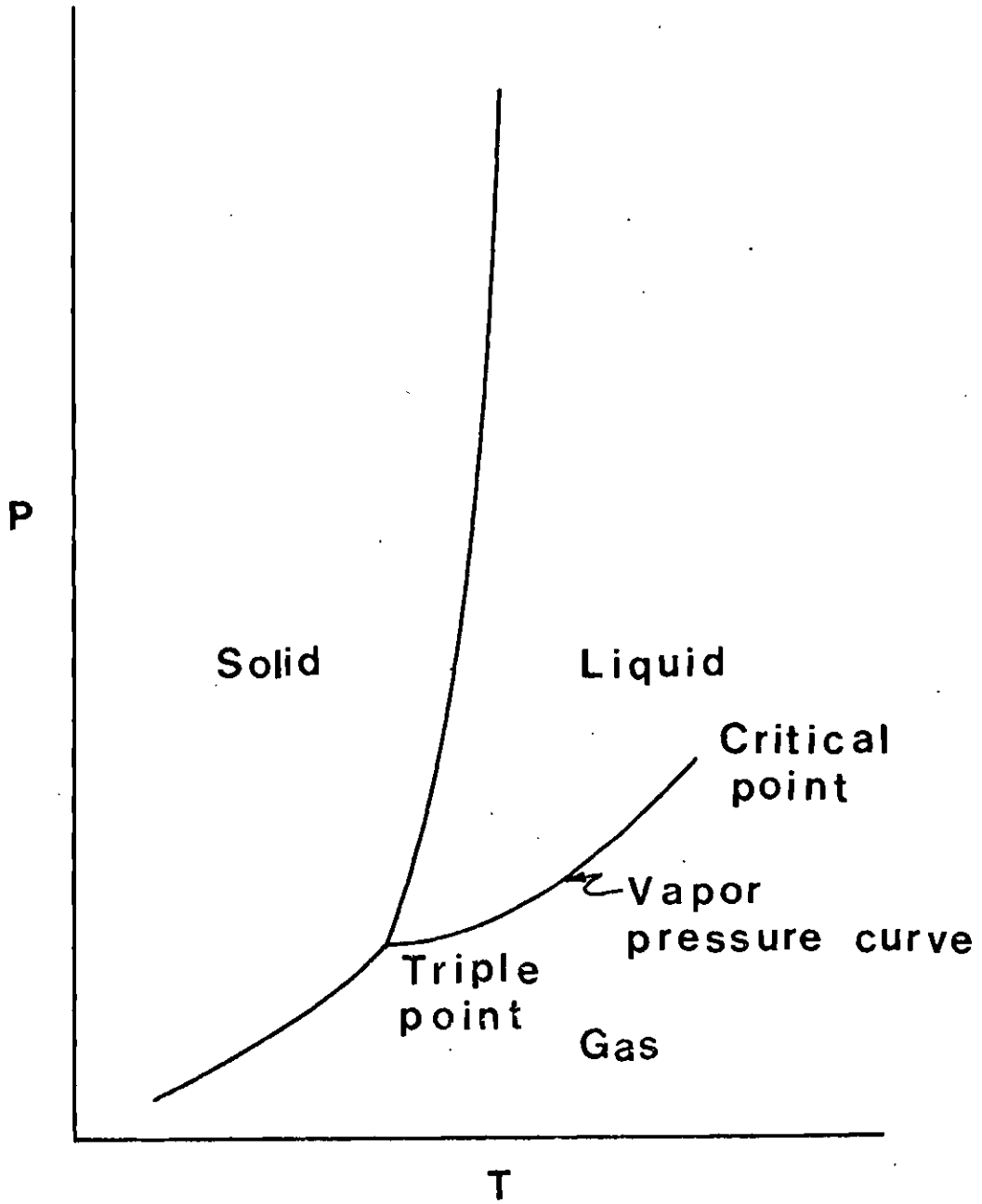


Figure 1. Pressure-Temperature Diagram for a Fluid

critical pressure is just the pressure at the critical temperature and density. For a fluid system above its critical temperature, in the absence of a gravitational field, the density is constant throughout the fluid. Below T_c the fluid separates into two phases with differing densities, the density difference increasing with decreasing temperature. This behavior is analogous to that of a magnetic system in which there is no spontaneous magnetization above the critical temperature. Below T_c there is spontaneous magnetization due to the alignment of the spins of the particles making up the system, an alignment that increases with decreasing temperature. Since the spontaneous magnetization is due to an ordering of the system, it may be defined as an order parameter that describes the system near the critical point. The order parameter is non-zero below the critical point, approaches zero as the critical point is approached from below, and is zero above the critical point. The corresponding quantity for the fluid system is the quantity $p = \rho - \rho_c$, the density difference between the gas or the liquid phase density and the critical density. Since there is no phase separation above the critical temperature, p is zero above the critical point and non-zero below. The importance of the order parameter is that it can be used to characterize the behavior of any system exhibiting a critical point.

The behavior of a fluid system may also be seen in Figure 2, in which the pressure as a function of density is presented for various values of temperature. The solid lines are isotherms, or lines of constant temperature. The dashed vertical line represents the critical isochore, the critical density of the fluid. For very high temper-

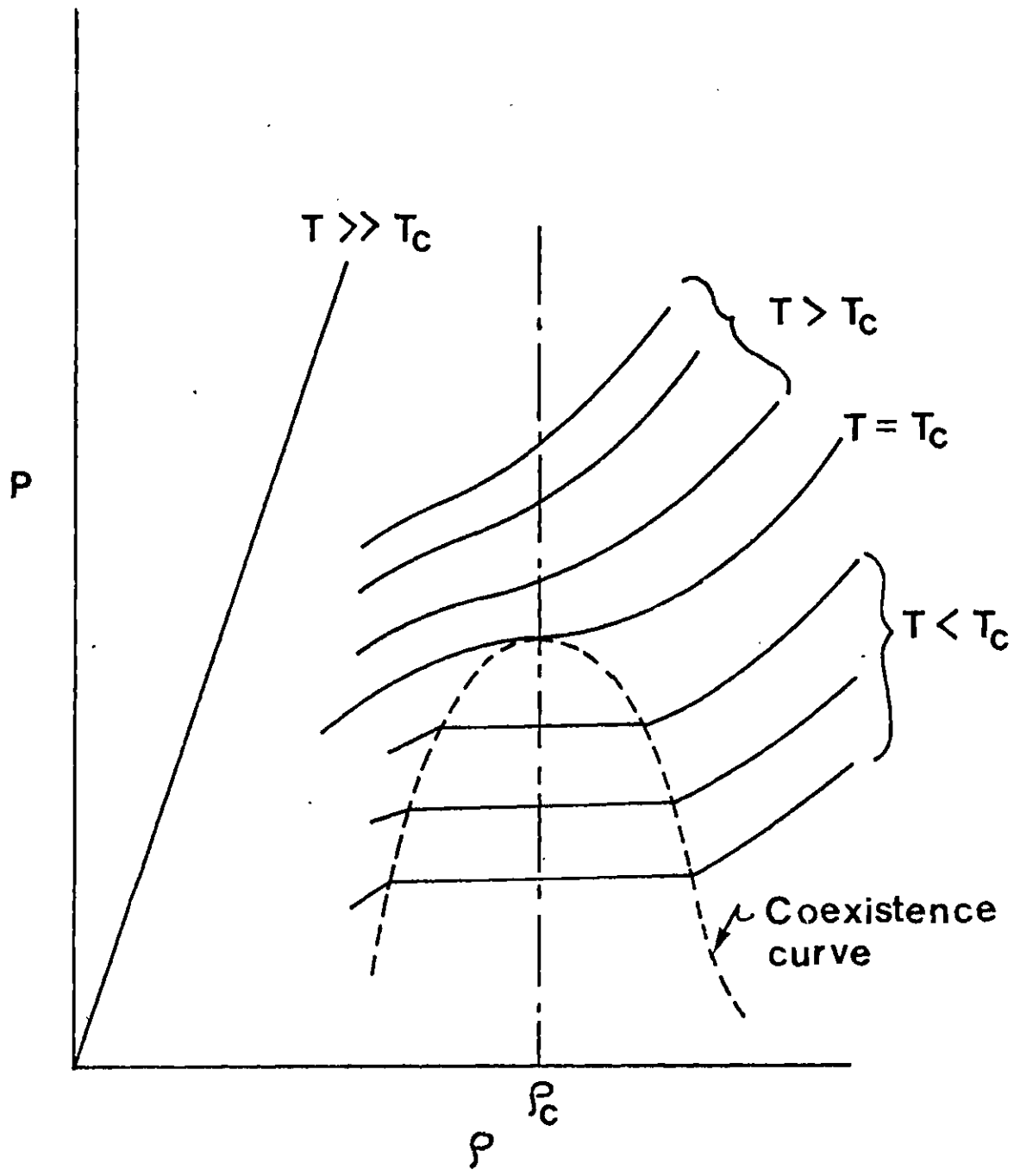


Figure 2: Pressure-Density Diagram of a Fluid in the Critical Region

atures, an increase in the pressure results in a proportional increase in the density, as expected from the ideal gas law. For lower temperatures, the isotherms are bent in the vicinity of the critical isochore indicating deviations from ideal behavior. Low temperature isotherms have a flat portion where the density can change without a corresponding change in the pressure. Physically, this corresponds to a transition from a completely gaseous to a completely liquid state; along the flat portion of the isotherm, the two phases coexist. The densities of the two coexisting phases at a particular temperature are the densities of the end points of the flat portion of the isotherm, and the curve drawn connecting these coexisting densities is known as the coexistence curve. The top of the coexistence curve, where the coexisting densities have become equal to the critical density, is the critical point. The isotherm passing through this point is the critical isotherm and is distinguished by the fact that its slope becomes zero at the critical point.

The isothermal compressibility κ_T of a fluid is defined as

$$\kappa_T = -\frac{1}{V} \left(\frac{\partial V}{\partial P} \right)_T = \frac{1}{\rho} \left(\frac{\partial \rho}{\partial P} \right)_T \quad 2-1$$

At the critical point the slope of the critical isotherm $\left(\frac{\partial P}{\partial \rho} \right)$ goes to zero and the isothermal compressibility diverges.

From Figure 2 it is apparent that two characteristics of the critical point are:

1. $\rho - \rho_c \rightarrow 0$ as $T \rightarrow T_c$ from below

2. $\kappa_T \rightarrow \infty$ as $T \rightarrow T_c$ from above on critical isochore
 or
 from below along coexistence curve

In addition to $\rho - \rho_c$ and κ_T , many of the properties that characterize a fluid either converge to zero or diverge at its critical point. In such cases, it is appropriate to describe the asymptotic behavior of a fluid property f , as $T \rightarrow T_c$ by a power law of the form:

$$f(\epsilon) \propto |\epsilon|^\lambda \quad \text{as } \epsilon \rightarrow 0$$

with ϵ defined as the reduced temperature

$$\epsilon = \frac{T - T_c}{T_c}$$

so that $|\epsilon|$ depends only on the relative temperature difference above or below the critical temperature. λ is the critical exponent for the power law and is defined precisely by the formula

$$\lambda = \lim_{\epsilon \rightarrow 0^\pm} \frac{\ln(f(\epsilon))}{\ln(\pm\epsilon)} \quad 2-2$$

as ϵ approaches zero from above (+) or below (-). With this definition, only the asymptotic behavior of the power law affects λ ; correction terms have no effect.

These critical exponents are important because they provide a numerical specification of critical behavior that may be verified by experiment or predicted by theory. They thus serve to facilitate com-

parison between various theories and with the experimental data. In the gas-liquid system the isothermal compressibility, the order parameter, the shape of the critical isotherm, the correlation length, and the specific heat all exhibit critical behavior.

Isothermal Compressibility

The isothermal compressibility is defined by Equation 2-1. As the critical temperature is approached from above on the critical isochore,

$$\kappa_T = \Gamma (\epsilon)^{-\gamma} \quad 2-3$$

As the critical temperature is approached from below on the coexistence curve,

$$\kappa_T = \Gamma' (-\epsilon)^{-\gamma'} \quad 2-4$$

γ and γ' are not necessarily equal, although there is experimental evidence that they are equal for CO_2 ⁷, and various theories predict such equality. The coefficients Γ , Γ' are not equal.

Coexistence Curve

The shape of the coexistence curve below T_c , and thus the behavior of the order parameter, is described by

$$p = (\rho - \rho_c) = B |\epsilon|^\beta \quad 2-5$$

β is the same whether ρ_c is approached from the gas or from the liquid side. Correction terms far from T_c result in the coexistence curve not being symmetrical on the gas and the liquid side; close to T_c however,

the coexistence curve is symmetric. A symmetric order parameter $p \propto |\epsilon|^\beta$ below T_c is a characteristic of critical phenomena in many systems, with β independent of the type of interaction (ferromagnetic, antiferromagnetic, or fluid) but depending only on the dimensionality and symmetry properties of the system.

Specific Heat

The change in temperature of a system for a given heat input at constant volume is given by

$$C_v = T \left(\frac{\partial S}{\partial T} \right)_v = \left(\frac{\partial U}{\partial T} \right)_v \quad 2-6$$

Although van der Waals and other classical theories did not predict a divergence in the specific heat, experimentally^{8,9} the specific heat is found to diverge slowly, possibly logarithmically. Close to the critical temperature, the specific heat C_v may be described by the following equation¹⁰

$$C_v = \frac{A}{\alpha} \left\{ |\epsilon|^{-\alpha} - 1 \right\} \quad \text{above } T_c \quad 2-7$$

$$C_v = \frac{A'}{\alpha'} \left\{ |\epsilon|^{-\alpha'} - 1 \right\} \quad \text{below } T_c \quad 2-8$$

As before, α may not be equal to α' . The divergence is written in a form having α in the denominator to take account of a possible logarithmic divergence in which α would equal zero. The above equations would then reduce to

$$C_v = -A \ln |\epsilon| \quad 2-9$$

Shape of Critical Isotherm

The slope of the critical isotherm is zero at the critical point, in accord with the fact that there is no lower temperature for which one phase can be in stable equilibrium at this density. Stability also requires that the second derivative be zero at this point. The rate at which the slope approaches zero is given by the critical exponent δ with the equation of the critical isotherm in the vicinity of the critical point given by¹¹

$$|P - P_c| \sim |\rho_L - \rho_G|^\delta \text{SGN}(\rho_L - \rho_G) \quad 2-10$$

$\text{sgn}(x) = +$ if x is positive, $= -$ if x is negative

Correlation Length

In any fluid, there will be fluctuations in density due to the random motion of the molecules of the fluid. Smoluchowski³ realized that the observed critical opalescence was due to light scattered by fluctuations that have become very large near the critical point. These large fluctuations can be described in terms of a correlation function and correlation length in the fluid and the light scattered by the fluid may be calculated in terms of the correlation function for the fluid.

The fluctuations may be described by assuming that a certain volume V of the fluid has an average number of particles, $\langle N \rangle$; in addition, particles may enter or leave the volume, so that the total number of particles may fluctuate about the average number. This results in density fluctuations in the element.

The fluctuation is denoted by $[N - \langle N \rangle] = \delta N$ and the mean square of the magnitude of the fluctuation, $\langle |\delta N|^2 \rangle$, is the measure of the amplitude of the fluctuation. This amplitude is related to the isothermal compressibility of the fluid by¹¹

$$\langle |\delta N|^2 \rangle = \langle N \rangle \frac{\kappa_T}{\kappa_{T_0}} \quad 2-11$$

κ_{T_0} is the isothermal compressibility of an ideal gas of non-interacting particles. According to 2-11, as the isothermal compressibility of the fluid diverges at the critical point, the amplitude of the fluctuations also diverges. The incompressible nature of the particles making up the fluid tends to limit the density increase in any small region of the fluid, so the amplitude increase must occur because many more particles are taking part in the fluctuation. The distance over which particles in the fluid can take part in a fluctuation is determined by the correlation length in the fluid. The number density of the fluid in a small region around a point \bar{r} may be defined as $n(\bar{r})$, with the fluctuation in the number density at a point \bar{r} equal to $[n(\bar{r}) - \langle n(\bar{r}) \rangle]$. A correlation function $G(\bar{r}, \bar{r}')$ relating the fluctuations at \bar{r} and \bar{r}' may be defined as

$$G(\bar{r}, \bar{r}') = \langle [n(\bar{r}) - \langle n(\bar{r}) \rangle] [n(\bar{r}') - \langle n(\bar{r}') \rangle] \rangle \quad 2-12$$

$G(\bar{r}, \bar{r}')$ may be thought of as being proportional to the conditional probability that if a fluctuation of a certain magnitude exists at \bar{r} there will be a like fluctuation at \bar{r}' . Since the fluid is uniform and

translationally invariant, the average density is the same throughout the fluid if the fluid is in one phase

$$\langle n(\bar{r}') \rangle = \langle n(\bar{r}) \rangle = \langle \frac{N}{V} \rangle = n$$

and $G(\bar{r}, \bar{r}')$ should depend only on the distance separating r and r' . $G(\bar{r}, \bar{r}')$ may then be written as $G(\bar{r}-\bar{r}')$ or $G(R)$, $R = |\bar{r}-\bar{r}'|$ with $G(r-r') = \langle n(r) n(r') \rangle - n^2$. As $R \rightarrow \infty$ the probability of finding a particle at r' should not be influenced by the presence or absence of a particle at r and the probabilities are independent:

$$\langle n(r)n(r') \rangle = \langle n(r) \rangle \langle n(r') \rangle = n^2$$

$G(R) \rightarrow 0$ then as $R \rightarrow \infty$. The range of R over which $G(R)$ is different from zero is the correlation length for the system.

From the definitions for G and N , one may obtain the relation¹¹

$$\langle |\delta N|^2 \rangle = \langle [N - \langle N \rangle]^2 \rangle = V \int G(R) dR \quad 2-13$$

Combining 2-11 and 2-13 one obtains

$$\frac{\kappa_T}{\kappa_{T_0}} = \frac{1}{n} \int G(R) d(R) \quad 2-14$$

$$n = \frac{\langle N \rangle}{V}$$

According to Equations 2-11 and 2-14 the magnitude of the density fluctuations as well as the isothermal compressibility are proportional to the integral of the correlation function over the range in which the correlation

function is non-zero. Since $G(R)$ is bounded above due to the incompressibility of the molecules making up the fluid, as the amplitude of the fluctuations diverges at the critical point, the correlation length must also diverge.

A form for the correlation function was given by Ornstein and Zernike⁵ who considered $G(R)$ as being due to a short range direct correlation that may be propagated from molecule to molecule resulting in a long range $G(R)$. This assumption led to a predicted form for the correlation function for large R

$$G(R) \propto \frac{e^{-K_1 R}}{R} \quad 2-15$$

K_1 determines the range of the correlation function. It has dimensions of inverse length, and its inverse $\xi = \frac{1}{K_1}$ is called the correlation length in the fluid. As the critical point is approached, the correlation length is found to diverge according to

$$\xi = \xi_0' |\epsilon|^{-\nu'} \quad \epsilon < 0 \quad 2-16$$

$$\xi = \xi_0' |\epsilon|^{-\nu} \quad \epsilon > 0 \quad 2-17$$

At the critical point, $K_1 = 0$, and the correlation function goes to zero as

$$G(R) \sim \frac{1}{R}$$

The ratio of the light scattered from some scattering volume dR with a

scattering vector k to that which would be scattered in the absence of fluctuations is given by the Fourier transform of the density correlation function defined in Equation 2-12

$$\frac{I(k)}{I_0(k)} \sim \int e^{-ik \cdot R} G(R) dR \sim \frac{1}{k^2 + K_1^2}$$

In the limit as $k \rightarrow 0$

$$\frac{I(0)}{I_0(0)} \sim \int G(R) dR \sim \frac{1}{K_1^2}$$

But this volume integral is equal to K_T/K_{T_0} by 2-14 so that

$$K_T \sim \frac{1}{K_1^2} = \xi^2$$

which implies that

$$2\nu = \gamma$$

for Ornstein-Zernike theory. More recently, Fisher¹⁰ has considered certain defects in Ornstein-Zernike theory and has proposed that the correlation function for large R be given by

$$G(R) \propto \frac{e^{-k_1 R}}{R^{1+\eta}}$$

Since the range far from the critical point is determined by K_1 , Fisher's correction would have no effect on the correlation length except very close to the critical point, and at the critical point the correlation function would go to zero as

$$\frac{1}{R^{1+\eta}}$$

η is a small number, probably slightly positive, but the value $\eta = 0$ is not excluded by present experimental evidence¹¹. Since experimental checks of Fisher's corrections to Ornstein-Zernike theory do not show any appreciable deviations from the predictions of Ornstein-Zernike theory for the temperature range considered in this experiment,^{12,13} the Ornstein-Zernike theory will be used to calculate the expected light scattering as a function of temperature for this experiment.

Theoretical Models of Critical Behavior

Van der Waals Model

The predictions of the various theories of critical behavior for fluids may be discussed in terms of the critical exponents defined previously, and the values of the exponents predicted by various theories may be compared with measured experimental values as a check on the validity of the theories. Historically, the first theory to have some success in describing the behavior of gases near their critical points was the van der Waals theory. The van der Waals equation of state may be written¹¹

$$\left(P + \frac{a}{\bar{V}^2}\right) (\bar{V} - b) = RT \quad 2-19$$

P = Pressure

R = $K \cdot$ (Avogadro's Number)

$\bar{V} = \frac{V}{n}$; a is a parameter which takes account of the attractive forces

between molecules; and b is a parameter taking account of the fact that the molecules behave as hard spheres. The isotherms predicted by the van der Waals theory are shown in Figure 3. Above and at T_c the isotherms are qualitatively correct, with a behavior indicating the divergence of the compressibility at the critical point. Below the critical temperature the isotherms are curved in such a way that the compressibility is negative for certain regions (B to C on labeled isotherm). This unphysical result implies that a decrease in the pressure should lead to an increase in the density. Also, the isotherms below T_c are characteristic of a single phase system and do not have the flat portion corresponding to a two phase system. The difficulty is removed by a free energy minimization argument, Maxwell construction, which shows that along a certain portion of the isotherms below T_c (between points A and D on Figure 3) the free energy is minimized if the system consists of coexisting liquid and gas phases rather than of one phase. This coexisting region is bounded by the coexistence curve. In addition to successfully describing the qualitative behavior of fluids near their critical points, van der Waals theory predicts that this behavior should be universal for all gases when the pressure, volume and temperature of a gas are expressed in terms of P_c , V_c , and T_c for the gas. This may be expressed by writing the van der Waals equation as

$$\left[\frac{P}{P_c} + \frac{3}{\left(\frac{v}{v_c}\right)^2} \right] \left[3 \left(\frac{v}{v_c}\right) - 1 \right] = 8 \frac{T}{T_c} \quad 2-20$$

with no explicit dependence on the parameters characteristic of the

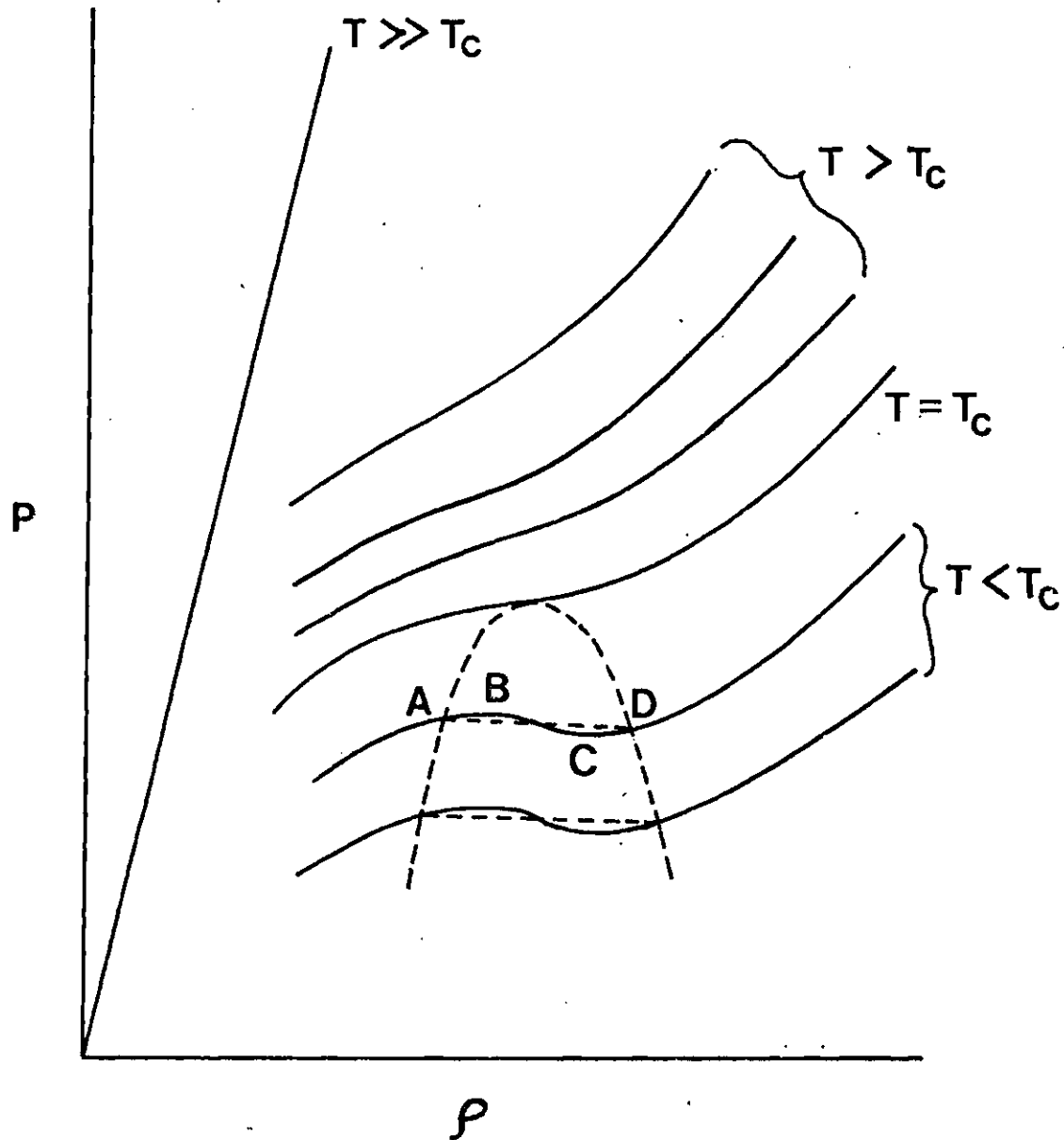


Figure 3. Van der Waals Isotherms for a Fluid

individual gas. This is known as the law of corresponding states and is thought to be valid for most gases near the critical point, although the van der Waals theory on which it is based does not hold in this region. The law of corresponding states has been used to determine the filling parameters for one of the gases investigated in this experiment.

When the van der Waals theory was used to predict values for the critical exponents, the predicted values were not in agreement with experimental results. The values expected for the various exponents on the basis of the van der Waals theory are given in Table 1. In particular, the van der Waals theory predicted that the specific heat would not diverge but the experimental evidence indicated that the specific heat was anomalously large and most likely divergent; in 1937 Michels, Blaisse, and Michels¹⁴ determined that the coexistence curve of CO₂ could best be fitted with $\beta = 0.35$ rather than $\beta = 0.5^2$. In 1945 Guggenheim¹⁵ analyzed data for eight simple gases and discovered that the coexistence curves of each could be fit to a simple power law with $\beta = 1/3$. The theories, Bragg-Williams and mean field, that have been developed to explain magnetic systems and alloys predicted the same values for the critical exponents as the van der Waals theory; so there were various classical theories that were qualitatively right but quantitatively wrong. Analysis of these theories showed that each contained, either explicitly or implicitly, a long range interaction. Various theoretical analyses have shown that the predictions of the van der Waals model follow rigorously from the assumption of long range forces²⁶.

Table 1. Selected Critical Point Exponents

	β	γ	α	δ	ν
Model Systems					
van der Waals (classical)	.5	1.0	0(discon.)	3	.5
D = 2 Ising Model	.125	1.75	0(log)	15	1
D = 3 Ising Model	.3125	1.25	.125	5	.638
Magnetic Systems					
Ni ¹⁶	.42	1.35	0	4.22	
EuS ¹⁶	.33		0.05		
Fluid Systems					
CO ₂ ^{17,18,19,20}	.345	1.17	.12		.63
A ²¹	.357	1.17			
He ^{4 22}	.354	1.14	.13	3.9	
Xe ^{23,24,25}	.35	1.3	.08	4.45	

Ising Model

The incorrect predictions of models with long range forces led to investigations of models with short range forces. The most fruitful of such models have been the Ising model for magnetic systems and the equivalent lattice gas model for fluid systems. The Ising model of a ferromagnet is characterized by the assumptions that each spin may have only two values and that there are only nearest neighbor interactions. The one dimensional Ising model does not exhibit a phase transition above absolute zero and so is only of limited interest. The two dimensional Ising model, solved by Onsagar²⁷ in 1944, has a non-zero critical point with associated critical exponents that may be determined in terms of the lattice parameters. The values for the exponents are shown in Table 1. This model predicted non-classical values for the exponents and the logarithmic divergency for the specific heat. In addition, calculations for various types of lattices and various types of interactions showed that these had no significant effect on the exponent values as long as the interaction was short range.

The three dimensional Ising model has not been solved exactly; however, various techniques have been developed to evaluate critical parameters associated with this model with a great deal of precision. Values for the exponents calculated for this model are also given in Table 1 as are experimental values for fluids and magnetic systems. The exponent values determined for fluids appear to be approximately the same as predicted by the three dimensional Ising model, but with consistent differences that appear to be greater than the experimental uncertainties in the determination of these quantities.

The two and three dimensional Ising predictions are not the same, and series calculations on the Ising model with dimensionality $D > 3$ indicate the results are strongly dependent on the dimensionality, approaching the classical values as $D \rightarrow \infty$. As the dimensionality becomes infinite, the number of particles that interact with each other directly becomes large even the interaction is short range. Thus the system becomes more like a classical system in which every particle is assumed to interact directly with every other particle.

Exponent Relationships

The physical parameters describing the behavior of a fluid are related through the thermodynamics of the system, and it is reasonable to expect that the exponents describing the behavior of these quantities near the critical point will also be related. Some of the relationships that connect the exponents are rigorously defined and others are conjectured with varying degrees of confidence. These serve to place limits on possible forms for an equation of state.

Two inequalities, the Griffiths and the Rushbrook inequalities, may be proved rigorously from general conditions of thermodynamic stability. These are:

$$\text{Griffiths Inequality}^{28} \quad \alpha' + \beta(1 + \delta) \geq 2$$

$$\text{Rushbrook Inequality}^{29} \quad \alpha' + 2\beta + \gamma' \geq 2$$

where α' is the critical exponent for the specific heat, β that for the coexistence curve, γ' for the isothermal compressibility, and δ for the critical isotherm as defined above.

Various other inequalities may be proved by making certain plau-

sible assumptions concerning the form of the thermodynamic potentials but have not been proved rigorously. Fisher³⁰ has obtained the Griffiths inequality as an equality by assuming a phenomenological Hamiltonian based on cluster theory. Widom³¹ found that for both classical theories and the two dimensional Ising model the equality

$$\gamma' = \beta(\delta-1)$$

is true. He conjectured that the relationship is a characteristic of all critical behavior.

Other equalities have been proposed. In general these equalities are satisfied by various model systems and are consistent with the available experimental evidence. Furthermore all may be derived from one set of assumptions, the scaling hypothesis, which describes time independent critical behavior in terms of only two independent parameters.

Scaling Laws

The scaling hypothesis may be described in terms of the Kadanoff picture¹⁶, which considers an Ising-like magnetic system whose behavior near the critical point may be thought of as being due to interactions between spins and the interactions between each spin and the external field. Close to the critical point, the spin-spin interactions will result in correlations extending over a very large number of spins. If the spin system is divided into cells, with each cell large compared to the individual spin site but small compared with the correlation length, the physical behavior near the critical point should be the same whether the interaction considered is spin-spin or cell-cell, or whether the

external field interacts with cells or with individual spins. The form of the correlation function should be the same in either case, with the only effect of a change in cell size being a change in the magnitude of the correlation function. That is, correlation functions considered for different cell sizes should differ only by some scale factor dependent on cell size. The interactions between spins and the external field should be determined by a relative field strength, h , while the spin-spin correlations should depend on the relative temperature ϵ of the system. The analogous parameters for the system considered as a cell system are \tilde{h} and $\tilde{\epsilon}$. As the field seen by a cell goes to zero, the field seen by a spin should also go to zero; the critical temperature should be independent of the cell size considered, and so the spin and the cell parameters should have the following relationship:

$$\tilde{h} = L^x h$$

$$\tilde{\epsilon} = L^y \epsilon, \quad L \text{ is the size of a cell}$$

x and y are arbitrary numbers

The functional form of the thermodynamic potentials also should not depend on the size of the cells considered; and the potentials for various cell sizes should be related by a constant of proportionality. The Gibbs potential, for example, may be written

$$G(\tilde{h}, \tilde{\epsilon}) = L^d G(h, \epsilon)$$

$$G(L^{\frac{x}{d}} h, L^{\frac{y}{d}} \epsilon) = LG(h, \epsilon)$$

The asymptotic behavior of the thermodynamic quantities obtained by

differentiating the potentials with respect to h or ϵ may be described in terms of the two parameters $\frac{x}{d}$ and $\frac{y}{d}$. The critical exponents may be defined in terms of these parameters, and a knowledge of the two parameters would be sufficient to determine all of the exponents. The scaling theory does not predict values for the parameters, however, and the usual practice is to measure any two of the exponents and to determine the others in terms of these two. The scaling predictions for exponent relationships are given in Table 2.

Universality

Since the forces involved in fluid and magnetic systems are of short range and the effects of critical phenomena are due to correlations involving many particles, the details of the interaction might be expected to have little effect on the critical behavior of the system. This concept is made more definite by saying that all systems of a given type, all fluids, or all magnetic systems of the same dimensionality, should have the same critical behavior; although for example, a fluid might be expected to have slightly different behavior from a three dimensional magnetic system. This law is an outgrowth of the law of corresponding states and is thought to be valid for fluid systems. The exponents β and δ have been measured for four fluids, CO_2 , Xe, He^4 , and H_2O , one of which, H_2O , is a polar molecule. The exponents are found to be the same ($\beta = .35$ and $\delta = 4.45$) in all cases²³. Since these two exponents are the same for the four fluids, the scaling theory requires that all of the exponents be the same, leading to $\gamma = 1.20$ and $\alpha = 0.1$. The value for α is approximately the same as that pre-

Table 2. Selected Exponent Relations from Scaling Laws

1. $\alpha = \alpha'$
2. $\gamma = \gamma'$
3. $\alpha + 2\beta + \gamma = 2$
4. $\gamma = \beta(\delta - 1)$
5. $\gamma' + \beta(1 - \delta) = 2$
6. $\alpha + \beta(\delta - 1) = 2$

dicted by the three dimensional Ising model and is supported by experimental values of $\alpha = 0.12$ for CO_2 ¹⁹ and $\alpha = 0.13$ for He^4 .²² The value for γ predicted by scaling theory is smaller than that predicted by the Ising model. It is consistent with, but slightly higher than, several recent experimental results: $\gamma = 1.17$ for CO_2 ,¹⁸ $\gamma = 1.17$ for Argon²¹, $\gamma = 1.18$ for krypton²¹, $\gamma = 1.14$ for He^4 .²² It is slightly lower than a value $\gamma = 1.225$ for SF_6 ³² and considerably lower than the $\gamma = 1.275$ reported for CClF_3 ,⁶ a polar fluid and one of the fluids investigated in this series of experiments. Earlier and presumably less accurate experiments have produced values for γ ranging between 1.0 and 1.37.

Polar Fluids

The above data indicates that the ideas of scaling and universality appear to be valid for simple gases; coexistence curve data indicates that β is experimentally measured to be the same even for polar fluids. The one series of experiments in which β has been measured for both polar and non-polar fluids¹⁷ shows a value for β that is larger for the polar fluid, but only by an amount that is approximately equal to the error reported in the measurement. The measurement of γ for CClF_3 is somewhat inconsistent with the value predicted by scaling as well as with measurements of γ for non-polar systems.

It is not clear that a permanent molecular dipole moment should affect the critical behavior of a fluid, but there is some evidence that such long range effects are important in other systems. According to Fisher, ferroelectric substances have critical points which are not closely analogous to those in fluid systems³², possibly due to the long

range Coulomb force. Gonzalo³³ has measured β and γ for triglycine sulphate, a ferroelectric material, and has obtained the values expected on the basis of classical theory. In addition, alkali metals, which are characterized by long range Coulomb forces, seem to have $\beta = 0.42-0.45$. One measurement of β for nickel, a ferromagnetic system for which long range dipole forces are important, shows a change in β from a value predicted by the Ising model to one closer to the classical value as the critical temperature is approached. Kadanoff has proposed that this may be due to magnetic dipole interactions¹⁶; there is disagreement about the experimental results, however.

It is desired in this series of experiments to measure the compressibility as a function of temperature and so to obtain γ for three polar fluids, N_2O , $CClF_3$, and CH_3F , ranging from the very slightly polar, N_2O , to the highly polar, CH_3F ; to determine whether the polarity of the fluids affects the measured values of γ ; and to measure values for ν to determine whether these polar molecules obey the scaling and universality laws that are applicable to simple fluids.

On the basis of these earlier experiments, it is thought that the effect of a dipole-dipole interaction should be a change in the measured exponent value from a value characteristic of Ising-like behavior to a value characteristic of classical behavior, either over the entire range measured, if the interaction is strong as in the ferroelectric materials, or at some characteristic temperature difference from the critical temperature if the interaction is relatively weaker as in the ferromagnetic materials.

Experimentally, however, a change in the measured value of the

exponent may be due to effects other than the dipole-dipole interaction. Such changes in slope may be distinguished from changes due to the dipole-dipole interaction in two ways. First, the change should be to a value close to the value expected on the basis of classical theory if the effect is due to the polar nature of the fluid. Second, an effect measured for one substance should also be observed on substances with greater polarity. For this reason, fluids with a range of dipole moments are investigated in this series of experiments. Any effect seen in the CClF_3 , for example, should also be seen in the CH_3F if the effect is due to the dipole-dipole interaction, since the dipole moment is considerably larger in the CH_3F than in the CClF_3 .

Measurements of Critical Behavior

Numerical measurements of critical behavior of fluids are obtained by measuring the quantities of interest as a function of the temperature difference from the critical point and determining the values of the exponent and the coefficient that best fit the experimental data. The specific heat is measured by the usual calorimetric methods. The co-existence curve is measured by determining the densities of the gas and the liquid phases as a function of temperature. The general behavior of the fluid in the critical region may be determined by mapping out the pressure, volume, and temperature relationships of the fluid, but common to each of these methods is the problem of density gradients in the fluid. These gradients arise because of the very large compressibility in the vicinity of the critical point and result in bulk measurements that average over a range of densities around the critical density and which,

consequently, may lead to inaccurate determinations of the critical behavior.

This difficulty may be minimized by the use of optical techniques. The index of refraction of the fluid may be measured and from this the density as a function of height may be determined very accurately by the use of the Lorentz-Lorenz relation¹⁷. In this manner the actual co-existing densities are measured rather than average values. Also, the intensity of the light scattered by a fluid is related to the compressibility and the correlation length in the fluid, so that a light scattering experiment may measure γ and ν . If a laser is used, the beam may be positioned so that it traverses the cell exactly at the critical density, again minimizing the problem of density gradients.

Light Scattering Equations for Fluids near Critical Points

Density fluctuations in fluids are related by the Lorentz-Lorenz formula to fluctuations in the polarizability and dielectric constant for the fluid, and these fluctuations are responsible for the light scattered by the fluid.

The fluid may be thought of as being divided into small volume elements (although each contains enough particles so that the fluid may be regarded as continuous). As the light passes through the fluid, a dipole moment is induced in each volume element. This moment is proportional to the electric field of the incident wave and oscillates with a frequency approximately equal to that of the incident wave (ω_0). As the dipole oscillates, it emits radiation. Although the fluids investigated

in this series of experiments are polar fluids, it is expected that the average dipole moment in any volume element will be zero and that the polarity of the material will not affect the light scattered from each volume element.

The discussion of the light scattering equations will follow a derivation of the light scattered from fluids near their critical points given by Benedek³⁴. The polarizability of each volume element may be divided into two parts: α_0 , an average polarizability, and $\delta\alpha$, fluctuations from the average polarizability. The average polarizability does not contribute to the light scattered except in transmission of the original beam through the fluid, so all of the light scattered out of the original beam is due to the fluctuations.

The scattering from each small volume element may be integrated over the scattering volume to obtain the total scattered E field, $E'(\bar{k}, t)$, at some point R with coordinates R, θ , ϕ , and φ as shown in Figure 4. The total scattered E field is:

$$E'(\bar{k}, t) = -E_0 \left(\frac{\omega_0}{c}\right)^2 \frac{e^{i(\bar{k} \cdot \bar{R} - \omega_0 t)}}{R} (2\pi)^{2/3} \sin \varphi \delta\alpha(\bar{k}, t) \hat{\varphi} \quad 2-21$$

E_0 is the magnitude of the E field of the incident beam, c the speed of light in a vacuum, φ the angle between the scattering vector k and the direction of polarization of the incident beam; $\hat{\varphi}$ is a unit vector as shown in Figure 3. The scattering vector k is related to the wave-vector k_0 of the incident beam by the following equation

$$k = 2k_0 \sin \frac{\theta}{2}$$

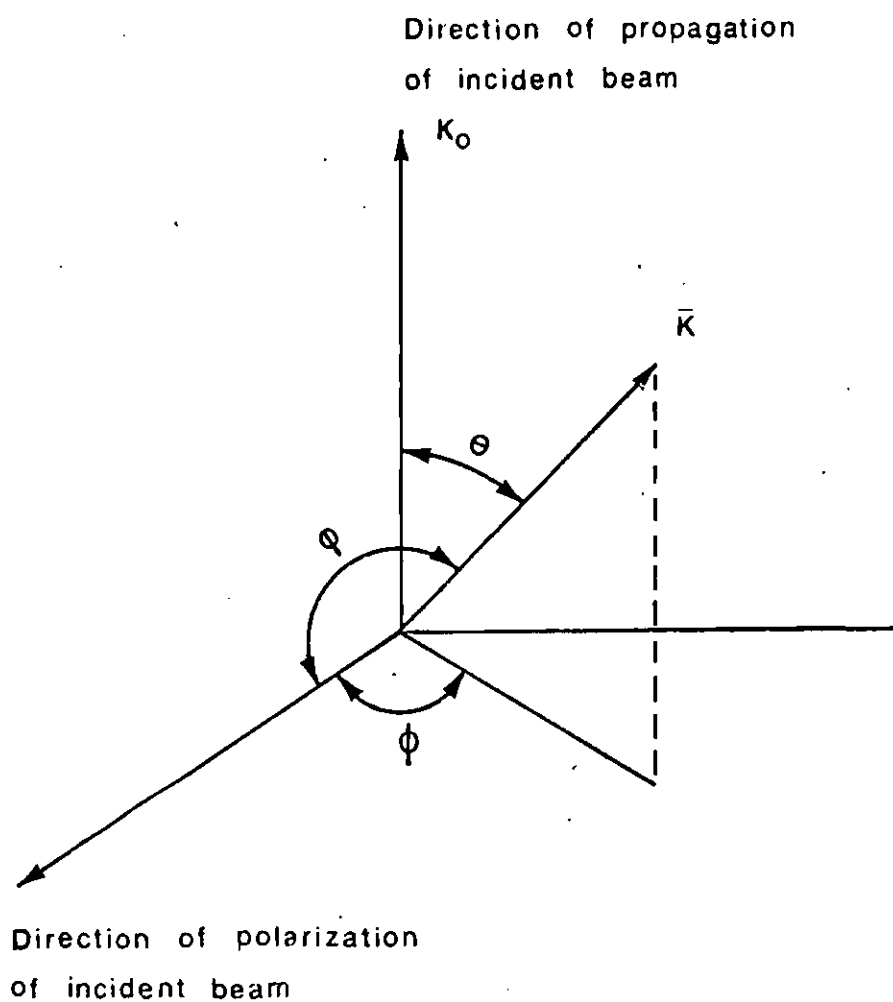


Figure 4. Definition of Angles Used
in Light Scattering Equations

with

$$k_o = \frac{2\pi}{\lambda_o}$$

λ_o is the wavelength of the incident radiation. Equation 2-21 assumes that there is negligible multiple scattering. Comparison of the cell size for this experiment with calculations of Swinney and Cummins³⁵ shows that this assumption is valid for $\Delta T > 0.1^\circ \text{C}$. In addition, the use of a small aperture limits the effect of multiple scattering still further. The fluctuation $\delta\alpha(\vec{k}, t)$ is the Fourier transform of the fluctuation in the polarizability $\delta\alpha(\vec{R}, t)$ which has the wavevector \vec{k} . The intensity of scattered radiation transmitted through a solid angle $d\Omega = \sin\theta d\theta d\phi$ about the scattering vector is given by Benedek as:

$$dI(\theta\phi) = \frac{c}{8\pi} \langle |E'(\vec{k}, t)|^2 \rangle R^2 d\Omega \quad 2-22$$

Using Equation 2-21 this can be written as

$$dI(\theta\phi) = \frac{cE_o^2}{8\pi} \left(\frac{2\pi}{\lambda_o}\right)^4 \frac{\pi}{2} \sin^2\phi \langle |\delta\epsilon(\vec{k}, t)|^2 \rangle d\Omega \quad 2-23$$

where we have substituted the dielectric constant fluctuation for the polarization fluctuation using the relationship:

$$\delta\epsilon(\vec{R}, t) = 4\pi\delta\alpha(\vec{R}, t)$$

obtained from the relation for dielectric materials,

$$\epsilon = 1 + 4\pi\alpha$$

which relates ϵ and α in a uniform dielectric medium³⁶.

According to Equation 2-23 the scattered intensity with scattering vector \bar{k} is determined by the mean square of the amplitude of the fluctuations in the dielectric constant with this wavevector. The magnitude may be calculated in terms of the thermodynamic variables of the system. In particular, since one wishes to measure the isothermal compressibility in the present series of experiments, it is natural to express the fluctuations in the dielectric constant ϵ in terms of the temperature and density fluctuations of the system. Fluctuations in ϵ may be written

$$\delta\epsilon(\bar{k}, t) = \left(\frac{\partial\epsilon}{\partial\rho}\right)_T \delta\rho + \left(\frac{\partial\epsilon}{\partial T}\right)_\rho \delta T \quad 2-24$$

A Fourier transform may be taken of each term to obtain the fluctuations in terms of the k dependence. The mean square average then becomes

$$\begin{aligned} \langle |\delta\epsilon(\bar{k}, t)|^2 \rangle &= \left(\frac{\partial\epsilon}{\partial T}\right)_\rho^2 \langle |\delta T(\bar{k}, t)|^2 \rangle + \left(\frac{\partial\epsilon}{\partial\rho}\right)_T \left(\frac{\partial\epsilon}{\partial T}\right)_\rho \\ &\quad \left[\langle \delta\rho(\bar{k}, t)\delta T(\bar{k}, t) \rangle + \text{Complex Conjugate} \right] \quad 2-25 \end{aligned}$$

ρ and T are statistically independent, so the third term is zero; and $\left(\frac{\partial\epsilon}{\partial T}\right)_\rho$ is considerably smaller than $\left(\frac{\partial\epsilon}{\partial\rho}\right)_T$ and may be neglected³⁷. The mean square fluctuation in the dielectric constant then depends on the mean square density fluctuation:

$$\langle |\delta\epsilon(\bar{k}, t)|^2 \rangle = \left(\frac{\partial\epsilon}{\partial\rho}\right)_T^2 \langle |\delta\rho(\bar{k}, t)|^2 \rangle \quad 2-26$$

The fluctuation $\delta\rho$ may be calculated by an analysis of the energy required to produce certain fluctuations. The probability of a fluctuation occurring is just

$$e^{-\frac{W}{kT}}$$

W is the work required to produce a given fluctuation, k is Boltzmann's constant. This work may be expressed in terms of changes in the thermodynamic variables, and since these variables have a Gaussian distribution, an average may be calculated. Far away from the critical point, as the correlation length $\rightarrow 0$, only the average density in a fluctuation need be considered, and the result calculated by Einstein in 1910⁴ is obtained:

$$\langle |\delta\rho(\mathbf{k}, t)|^2 \rangle = \frac{V}{(2\pi)^3} \kappa_T kT \quad 2-27$$

Closer to the critical point, the energy of the fluctuation will depend on the gradient of the particle spacing as well as on the average density in a fluctuation. That is, the fluctuations can no longer be considered to be independent of one another, but the correlations between functions must be taken into account. When the correlation function $G(R)$ discussed previously is included, the Einstein result is modified and becomes

$$\langle |\delta\rho(\bar{\mathbf{k}}, t)|^2 \rangle = \frac{\kappa_T kT \rho^2}{1 + \xi^2 k^2} \frac{V}{(2\pi)^3} \quad 2-28$$

Where ξ is the correlation length defined previously. This result was obtained by Ornstein and Zernike in 1914⁵.

The mean square average may also be calculated using Fisher's modified correlation function to obtain

$$\langle |\delta\rho(k, t)|^2 \rangle = \frac{\kappa_T kT \rho^2}{(1 + \xi^2 k^2)^{1 - \frac{1}{2}\eta}} \cdot \frac{V}{(2\pi)^3}, \quad 2-29$$

with η the critical exponent describing Fisher's modification of Ornstein-Zernike theory. As before, a small non-zero value for η will not affect the calculated values for the scattered intensity in this experiment; and the Ornstein-Zernike result will be used for the data analysis.

The final value for the intensity of light scattered through some $d\Omega$ about a scattering vector k per unit path length in the scattering volume is

$$dI(\theta, \phi, \varphi) = I_0 \left(\frac{2\pi}{\lambda_0} \right)^4 \left[\rho \frac{\partial \epsilon}{\partial \rho} \right]^2 \kappa_T \frac{kT \sin^2 \varphi}{1 + (k\xi)^2} d\Omega \quad 2-30$$

which reduces to

$$dI(\theta, \phi, \varphi) = I_0 \left(\frac{2\pi}{\lambda_0} \right)^4 \left[\rho \frac{\partial \epsilon}{\partial \rho} \right]^2 \kappa_T kT \sin^2 \varphi d\Omega \quad 2-31$$

as $\xi \rightarrow 0$.

$\frac{I_0}{A} = \frac{CE_0^2}{8\pi}$ and $V = L \cdot A$, $L =$ path length in the scattering volume. The relative intensity per unit path length may be obtained by integrating 2-30 over all angles.

$$I_{\text{tot}} = \int_{\phi=0}^{2\pi} \int_{\theta=0}^{\pi} dI(\theta, \phi) \sin^2 \phi \sin \theta \, d\theta \, d\phi$$

$$\frac{I_{\text{tot}}}{I_0} = \frac{\pi^3}{\lambda_0^4} \left(\rho \frac{\partial \epsilon}{\partial \rho} \right)^2 kT \kappa_T \left[\left(\frac{2\alpha^2 + 2\alpha + 1}{\alpha^3} \right) \ln(1 + 2\alpha) - \frac{2(1 + \alpha)}{\alpha^2} \right] \quad 2-32$$

where $\alpha = 2(k_0 \xi)^2$, a dimensionless parameter. Equation 2-32 may be written as

$$\frac{I_{\text{tot}}}{I_0} = \frac{\pi^3}{\lambda_0^4} \left(\rho \frac{\partial \epsilon}{\partial \rho} \right)^2 kT \kappa_T f(\alpha) \quad 2-33$$

$$f(\alpha) = \left[\frac{(2\alpha^2 + 2\alpha + 1)}{\alpha^3} \ln(1 + 2\alpha) - \frac{2(1 + 2\alpha)}{\alpha^2} \right]. \quad 2-34$$

As $\xi \rightarrow 0$, $f(\alpha) \rightarrow 8/3$, and for this limiting case, the total relative scattered intensity becomes:

$$\frac{I_{\text{tot}}}{I_0} = \frac{8}{3} \frac{\pi^3}{\lambda_0^4} \left[\rho \left(\frac{\partial \epsilon}{\partial \rho} \right) \right]^2 kT \kappa_T \quad 2-35$$

This equation is the same as that which is obtained if Equation 2-31 is integrated over all angles. Comparison with measured values for the correlation length in other fluids near the critical point indicates that Equation 2-35 is a good approximation for temperatures more than 0.5°C away from the critical point.

The isothermal compressibility may be determined using Equation 2-35. λ_0 , kT , and ρ are all known; $\frac{\partial \epsilon}{\partial \rho}$ may be determined from measured

values of the index of refraction and the use of the Lorentz-Lorenz relation. Each of these quantities, except for the temperature, is a constant for each sample during this experiment. The temperature dependence due to T is small over the range of temperatures encountered during this series of experiments and may be removed entirely by multiplying both sides of Equation 2-35 by (T_c/T) , which then may be written in the form:

$$\frac{I_{\text{tot}}}{I_0} = C K_T \quad . \quad 2-36$$

C is a constant determined by evaluating the parameters for each substance.

The total scattered intensity may be determined by measuring the attenuation of light passing through the sample cell. The attenuation of light of intensity I per unit length in the sample cell is given by Kerker³⁶, although with slightly different notation, as

$$-\frac{dI}{dx} = \left(\frac{I_{\text{tot}}}{I_0}\right) I$$

x = path length

which may be solved to obtain

$$I_t = I_0 e^{-\left(\frac{I_{\text{tot}}}{I_0}\right) L} \quad 2-37$$

I_t the transmitted beam, I_0 the incident beam, L total path length. The quantity $\left(\frac{I_{\text{tot}}}{I_0}\right)$ is seen from Equation 2-37 to be an attenuation or ex-

inction coefficient and is called the turbidity of the fluid:

$$\tau = \frac{I_{\text{tot}}}{I_0} .$$

τ may be determined from a measurement of the incident and transmitted beams by means of the equation

$$\tau = - \frac{1}{L} \ln \frac{I}{I_0} \quad 2-38$$

with L the path length in the scattering cell. The usual dimensions for turbidity are $(\text{cm})^{-1}$ and common values for the turbidity in ordinary liquids range from $4 \times 10^{-3} \text{ cm}^{-1}$ to $2 \times 10^{-4} \text{ cm}^{-1}$, with most liquids near the lower end of the range. The turbidities near the critical point are considerably higher, with $\tau \approx 10^{-2}$ at $\Delta T = 1^\circ \text{ C}$ ranging to $\tau \approx 1$ a few hundredths of a degree from the critical point.

With this definition of turbidity, Equation 2-36 may be written in the form

$$\tau = C \cdot \kappa_T \quad 2-39$$

with the measured τ related by a constant of proportionality to the isothermal compressibility for temperatures greater than 0.2° away from the critical point.

Determination of Γ, γ

From the previous discussion of critical exponents, κ_T should have the form

$$\kappa_T = \Gamma \epsilon^{-\gamma}$$

near the critical point. This functional form for χ_T may be inserted into Equation 2-39 to obtain

$$\tau = C \Gamma \epsilon^{-\gamma} \quad 2-40$$

which may be written

$$\frac{\tau}{C} = \Gamma \epsilon^{-\gamma} \quad 2-41$$

In this series of experiments, τ is measured as a function of the temperature difference from the critical temperature. These measured values of τ as a function of the reduced temperature ($\epsilon = \frac{\Delta T}{T_C}$) may then be fit to a function of the form

$$(C \Gamma) \epsilon^{-\gamma} \quad 2-42$$

using a generalized least squares fitting routine. $(C\Gamma)$ and γ are treated as adjustable parameters and are varied by the routine in order to obtain a best least squares fit. $(C\Gamma)$ is then divided by C to determine Γ . In addition the measured values of the turbidity may be adjusted as described in the next chapter to minimize the errors in Γ and γ . In this way the magnitude of the isothermal compressibility as a function of temperature, as well as the critical exponent describing the asymptotic temperature dependence may be determined.

Determination of ξ_0 and ν

The correlation length ξ as a function of temperature may also be determined. After values for Γ and γ have been calculated, these values

may be substituted into Equation 2-40; all of the terms on the right hand side of this equation, as well as Equation 2-35, are then known. These known quantities with a temperature dependence given by γ may be designated as τ_0 , the turbidity that would be measured at any temperature close to the critical point in the absence of correlation effects. Equation 2-33 may then be written

$$\tau = \tau_0 f(\alpha) \quad 2-43$$

which may be put into the form:

$$f(\alpha) - \frac{\tau}{\tau_0} = 0 \quad 2-44$$

with τ the measured turbidity at some ΔT . ξ may be calculated from Equation 2-44 because at a particular temperature the turbidity is measured, τ_0 is calculated from a knowledge of Γ and γ ; and so Equation 2-39 is of the form

$$f(\alpha) - (\text{CONST}) = 0 \quad 2-45$$

Equation 2-45 may be solved numerically to determine α , and since $\alpha = 2(k_0 \xi)$, the correlation length at a particular temperature may be determined. The procedure is then repeated for other temperatures.

The functional form of the correlation length near the critical point is given by Equation 2-17 as

$$\xi = \xi_0 \epsilon^{-\nu} \quad 2-46$$

The measured values of ξ as a function of temperature are then fit to a function of this form with a generalized least squares fit with ξ_0 and ν considered as adjustable parameters.

Summary of Data Analysis

To summarize, the procedure used in the analysis of the data is the following: The turbidity data is fit to Equation 2-41 in the temperature region in which the correlation length may be assumed to be zero, and Γ and ν are determined. These values for the isothermal compressibility are then substituted into Equation 2-35 in which, with the measured value of turbidity, the only unknown is a function of the correlation length. This equation is solved for several data points to obtain the correlation length for various temperatures. These values for ξ are then fit to Equation 2-46 to determine ξ_0 and ν .

CHAPTER III

EXPERIMENTAL APPARATUS AND PROCEDURES

Properties of Sample Fluids

Three substances were selected for this investigation, nitrous oxide (N_2O), methyl fluoride (CH_3F), and chlorotrifluoromethane (Freon 13, $CClF_3$). Each is a polar fluid; each has a "convenient" critical temperature slightly above room temperature; all are non-toxic. The coexistence curves and critical temperatures and densities are known for two of these substances, N_2O and $CClF_3$ ³⁸. The critical behavior of CH_3F has not been investigated recently and no reliable data on its critical properties are available.

The gases used in this investigation were obtained from Matheson Gas Products, and no attempt was made to further purify them. N_2O has a minimum purity of 98%, the principal impurity being air. The method of filling the cell by condensation indicated that the purity of the nitrous oxide in the cell was greater than that in the cylinder. Comparison of the critical temperature obtained from this experiment and critical temperatures determined for N_2O with carefully controlled amounts of impurities¹⁷ indicates that impurities in the present sample of N_2O are considerably less than that specified by the Matheson Gas Products. Furthermore, the analysis in reference (17) of the coexistence curve data for N_2O indicates that the prime effect of impurities of the order of 1% is a change in the critical temperature T_c , with

only a slight effect on the critical exponent β . Both CClF_3 and CH_3F are 99% pure, the principal impurities being air for CClF_3 and silicon tetrafluoride and dimethyl ether for CH_3F .

N_2O is a linear molecule with an N-O bond distance of 1.185 Å and an N-N bond distance of 1.128 Å. The CH_3F molecule is a methane-like molecule in which one of the hydrogen atoms has been replaced with a fluorine atom, distorting the original tetrahedral symmetry. The C-F bond distance is 1.3852 Å and the C-H bond distance is 1.06 Å. The H-C-H angle is $109^\circ 50'$. CClF_3 is also a methane-like molecule in which three of the hydrogen atoms have been replaced by fluorine atoms and the fourth by a chlorine atom. The C-F bond distance is 1.328 Å and the C-Cl bond distance is 1.751 Å. The F-C-F bond angle is $108.6^\circ \pm .4^\circ$.

The dipole moments for these gases are: .17 D for N_2O , .50 D for CClF_3 , 1.856 D for CH_3F ³⁹. Some of the previously reported critical data for these gases is summarized in Table 6.

Sample Preparation

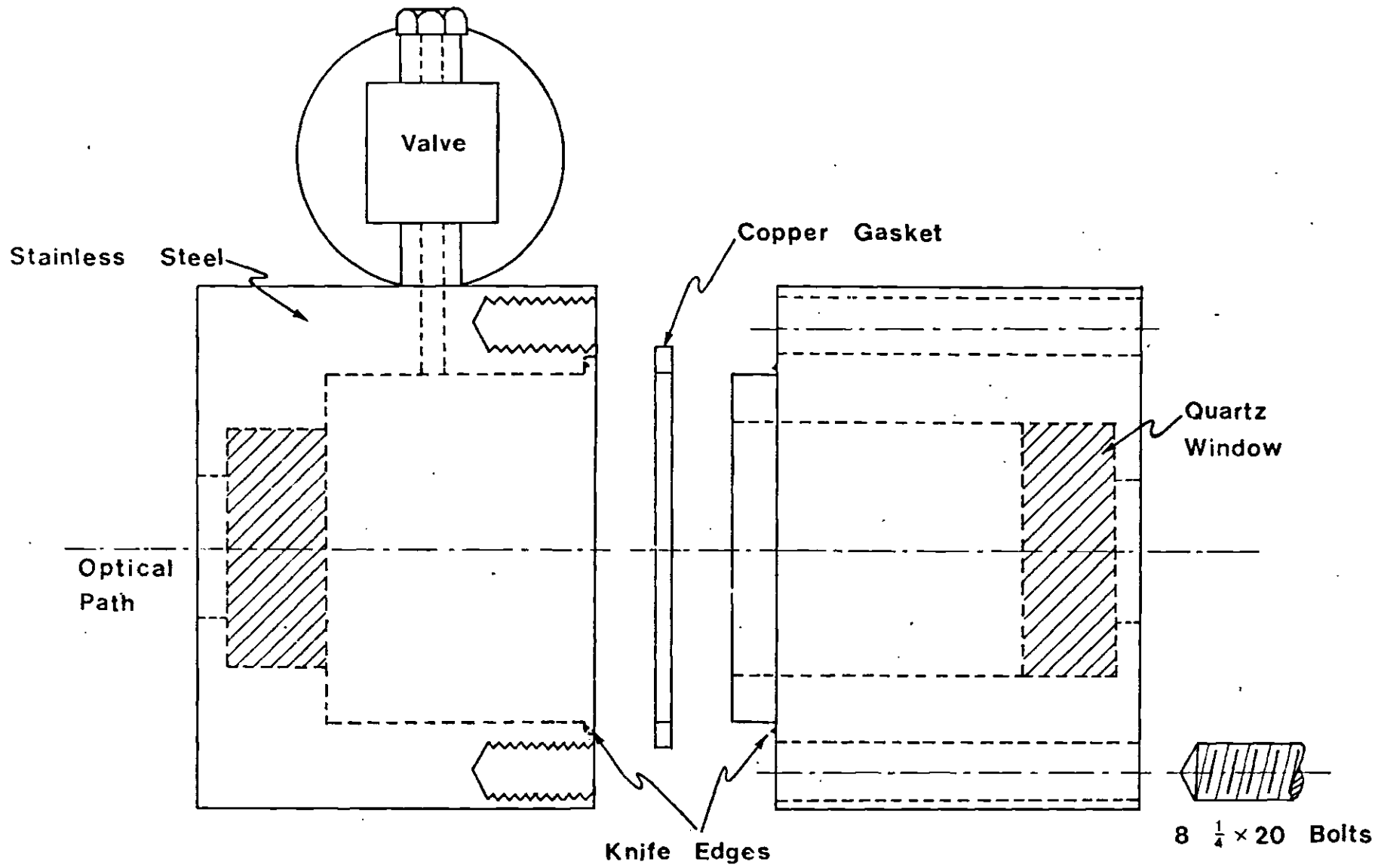
Cell Design

The critical pressures of these fluids are fairly high, ranging from 38 to 72 atm, as shown in Table 6. To contain this pressure, the fluids must be retained in a suitable sample cell. There are two general approaches to a design of a sample cell to be used in critical point investigations. One is a glass cell which is sealed off with a flame after filling; the other is a metal cell, generally of stainless steel, with optical windows. The advantage of the metal cell is the

ease of adjusting the amount of fluid in the cell through a valve connection. Also, since a turbidity measurement requires a cell with a fairly long optical path length and flat ends, a metal cell will contain the pressure with greater safety.

Although there are minor differences between the cells used for the different fluids, the design, shown in an exploded diagram in Figure 5, is basically that of the cell for N_2O . This design is adapted from a design of Morey and Fenner⁴⁰ which has been modified with slightly different sealing geometry and with the addition of windows for optical measurements. The construction of each is of stainless steel with $\frac{1}{2}$ " thick fused quartz windows, with each cell having an optical path length of approximately 38 mm. Thick windows are required because of the enormous amount of stress on the unsupported area of the window. The stress is inversely proportional to the square of the thickness⁴¹ and approaches the failure point of the quartz if thinner windows are used. Although the rated tensile strength of the quartz is not exceeded when $\frac{1}{4}$ " thick windows are used, any unevenness in the supporting area of the window can cause greater stresses, resulting in cracking of the window. On a filling attempt with $\frac{1}{4}$ " windows, one of the windows failed at a pressure of approximately 900 psi. A calculation that determines the stress on a window of given size and thickness is given in Appendix A.

When uncoated quartz discs were used in the cell containing the methyl fluoride, etching of the interior surfaces of the windows occurred. This etching was eliminated by coating the interior surfaces of the windows with 350 cs Dow Corning 200 fluid (a dimethylsiloxane



Scale Approximately Full Size

Figure 5. Exploded View of High Pressure Cell

polymer) and baking for 3 hours at 350° C. The windows used in the other two sample cells were uncoated.

Each of the windows sits in a well and is supported over $\frac{1}{2}$ of its area by the shoulder of the sample cell. The well in which the windows are seated is drilled 4 to 6 thousandths of an inch oversize, to assure that the differential contraction on cooling will not crack the windows. The actual seal of the window to the cell is made with a low viscosity epoxy, TRACON TYPE 2114 that flows and completely fills the space between the window and the shoulder. When the interior of the cell is pressurized, the internal pressure pushes the window toward the shoulder, thereby improving the contact between quartz, metal, and epoxy.

The cell is constructed in two sections joined after the windows are seated from the inside. The two sections are joined together by eight $\frac{1}{4}$ " bolts. The high pressure seal consists of knife edges machined onto a shoulder of each section of the sample cell and a copper gasket into which the knife edges impress when the two sections are drawn together by tightening the bolts. The valve used in this sample cell is a Nupro Model 4H stainless steel bellows valve joined to the body of the sample cell with a silver solder seal; the valve has a pressure rating of 1000 psi.

The entire sample cell assembly is supported by a rigid framework and is suspended by a $\frac{1}{4}$ " steel rod from a Brinkmann cell holder that may be adjusted to give a rotational motion about the vertical axis and translational motion in the vertical direction. This latter capability is necessary to enable the cell to be positioned accurately so that the

beam passes through the sample at the critical density.

Determination of Cell Volume

To determine the critical density of each of the samples used in this experiment the volume of each of the cells must be known precisely. To achieve this the empty cell was weighed, filled with water, and weighed again using the density of water to determine the volume. To fill the cell it was necessary to evacuate the cell through one arm of a two position stopcock connected to the sample cell. The other arm was connected to a water reservoir and the line to the vacuum pump was opened and the cell pumped out. The stopcock valve was then turned to open the line to the water reservoir, and the water flowed into the cell. The procedure was repeated until all the air bubbles present in the cell were removed.

This method involved two major sources for uncertainty. First, the mass of the sample cell is approximately 1800 gms and the available balances with the required capacity have an accuracy no better than 0.1 gms. Secondly, water wets the steel and the glass poorly, causing bubbles to be formed. In the cells used for N_2O and CH_3F , the opening into the valve was small; there is the possibility that the space was not completely filled with water. This volume is approximately 1 cc and introduces an uncertainty into the volume determination of these cylinders. The cell used for $CClF_3$ has a larger opening so that this uncertainty is not present. A calculation for the volume of the cell containing the N_2O is presented in Table 3; the calculations for the other cells are analogous.

Table 3. Determination of Sample Cell Volume of
the N₂O High Pressure Cell

Empty wt. of cell	1818.3 gms 1818.4 gms 1818.4 gms
Avg. wt.	1818.4 ± 0.1 gms
Filled wt. of cell	1871.1 gms 1870.9 gms 1871.0 gms
Avg. wt.	1871.0 ± 0.1 gms
2nd trial filled	1871.0 gms 1871.0 gms
Avg. wt.	1871.1 ± 0.1 gms
Avg. of two trials	1871.0 ± 0.1 gms
Mass of water in cell	52.6 ± 0.2 gms
Volume of water present	52.6 ± 0.2 cm ³
Possible additional volume	1.1 ± 0.2 cm ³
Limits on the volume:	Max. vol. 54.1 cm ³ Min. vol. 52.4 cm ³
Avg. of these two numbers	53.3 cm ³
Vol. for this cell	53.3 ± 0.8 cm ³

Cleaning of Cell

The cells were first degreased by immersion in trichloroethylene vapor. The interior of the cell was then washed with acetone followed by methanol. After the washing and before sealing the cell, methanol was vaporized, then condensed on the interior of the cell and allowed to run off, removing any dust particles that may have settled on the surface.

Calculation of Filling Parameters

Before filling the cell, it is necessary to determine the amount of gas needed for the sample to be at its critical density. The mass needed is determined from the measured volume of the cell and the critical density from Table 6. The amount needed to fill the cell is calculated in terms of the pressure difference for each gas, assuming ideal behavior, and a correction is made for the deviation of the gas from ideal behavior. The amount actually condensed depends on the pressure difference in the gas handling system before and after filling and the mass of gas present in the system for a given pressure.

The density of each gas at standard conditions is found in the Matheson Gas Data Book⁴², and a correction is applied for given room conditions. This density is multiplied by the volume of the gas handling system to determine the mass of the gas in the system at a pressure of 1 atm. Assuming ideal behavior, this same mass of gas will be present for each atmosphere of pressure present in the system; since the total mass needed is known, this mass may be expressed in terms of a pressure difference in the gas handling system before and after filling. A sample calculation for N₂O is given in Table 4.

Table 4. Calculation of Filling Parameters for N₂O Cell

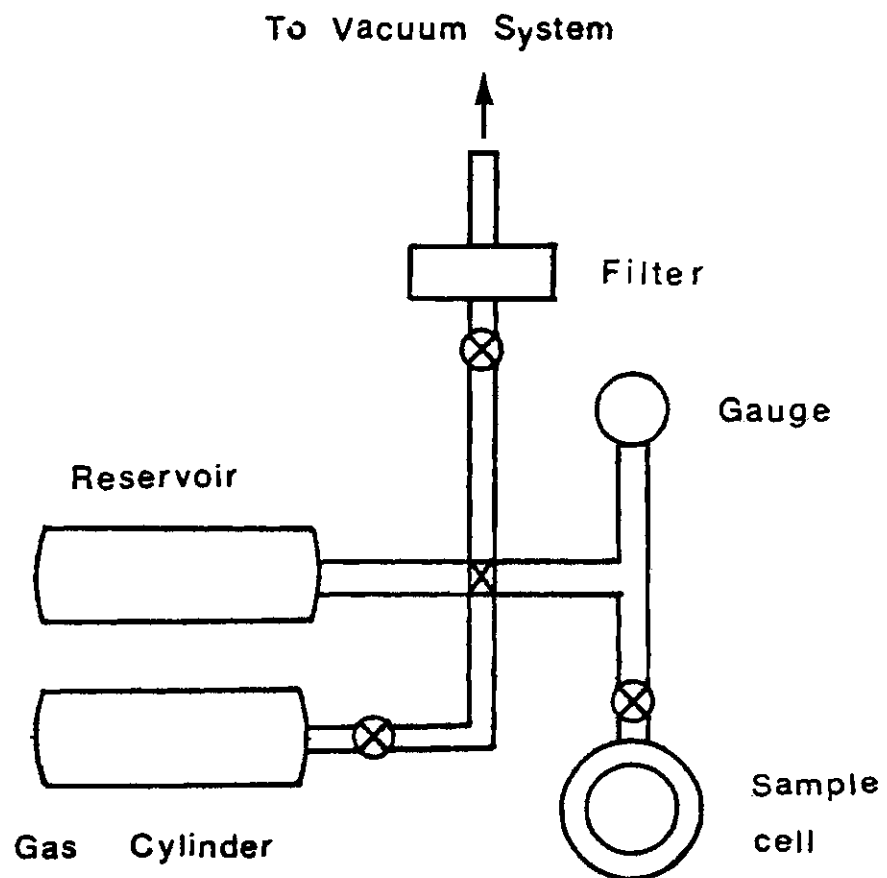
Critical density	= .452 g/ml
Volume of sample cell	= 53.3 ml
Mass needed for critical density in cell	= 24.1 gms
Density of gas 0° C, 1 atm	= 1.997 g/liter
Density at 18° C, 1 atm	= 1.87 g/liter
Volume of gas handling system	= 340 ml
Mass in system at 18° C, 1 atm	= .637 gms
Number of atm to fill cell (if ideal)	= 37.82
Number of psi difference	= 556

In fact, the density is greater than the ideal density at high pressures. While data are not tabulated in the International Critical Tables for N_2O or the other gases that are the subjects of this investigation, the density for CO_2 , which has a similar critical behavior, is about 10% higher than corresponding ideal density at 250 psi⁴³. The exact amount is non-critical, since the amount of the gas in the sample cell may be adjusted by valving gas out or by condensing more gas in.

Filling of Cell

After the cell was cleaned and sealed, and after a calculation of the filling parameters was made, the cell was placed in an oven and attached to a vacuum system. As the cell was pumped out, the oven was heated to approximately 50° C to outgas water from the interior surfaces. After several hours in the oven no change in the pressure of the vacuum system was observed when the cell valve was closed or when it was re-opened, indicating that the outgassing had been accomplished. The cell valve was then closed and the cell removed from the vacuum system and connected to the gas handling system, shown in Figure 6, which was then connected to the vacuum system. The gas handling system was pumped out to about 50 microns and the sample cell valve opened. Pumping out continued overnight.

As the first step in the actual filling procedure, the sample cell valve is closed and the sample cell immersed in a slurry of dry ice, water, and isopropyl alcohol and cooled to approximately -30° C. The relative amount of water and of alcohol is determined by the requirement that the temperature of the cell not go below -50° C. Below this temperature the epoxy fails. After the cell has cooled to approx-



⊗ indicates valve

Figure 6. Filling System for Sample Cell

imately the temperature of the slurry, the valve between the gas handling system and the vacuum system is closed and the valve to the gas bottle is opened. Gas flows into the gas handling system until the pressure reaches 400 psi, maximum pressure of the gauge, at which time the gas valve is closed and the sample cell is opened. A portion of the gas condenses into the cell, and the pressure in the system drops until it is equal to the vapor pressure of the liquid in the cooled cell. If calculation shows that the initial pressure required is greater than 400 psi, the filling procedure may be repeated. Usually, not enough of the gas will be condensed on one condensation, so the valve to the cell must be closed, more gas introduced into the gas handling system, and condensed into the cell. After the calculated amount of gas has condensed, the valve is closed, and the slurry is removed from around the cell.

Determination of Critical Fill

Above the critical temperature the average density is just the density of the one phase fluid; below the critical temperature the density of each phase varies with temperature along the coexistence curve. The average density remains constant as long as the cell is sealed, and the volume of each phase varies as the critical temperature is approached. When the average density is equal to the critical density, the volumes of the liquid and of the gas phases will be constant and equal to each other as the critical temperature is approached from below. This equality of volume of the liquid and gas phases is used to determine that the fluid in the cell is at its critical density.

The volume of the liquid phase relative to the total volume of

the sample cell below the critical temperature is given by Equation 3-1 (for derivation see Appendix B):

$$\frac{V_L}{V} = \frac{\rho - \rho_c}{2 B_1 \rho_c \epsilon^\beta} + \frac{1}{2} . \quad 3-1$$

V is the total volume of the sample cell, V_L is the volume of the liquid, ϵ the reduced temperature, ρ the average density of the fluid in the cell, ρ_c the critical density. B_1 and β describe the shape of the coexistence curve.

According to Equation 3-1, for densities greater than the critical density, as the critical temperature is approached from below, the volume of the liquid phase increases. Eventually as $\epsilon \rightarrow 0$ there will be some temperature at which $V_L = V$ and the fluid in the cell will be entirely in the liquid phase. Experimentally, the meniscus, the line marking the boundary between the two phases, appears to rise and finally to go through the top of the cell. The temperature at which this occurs is the temperature at which the density of the liquid on the coexistence curve equals the average density inside the cell. For densities less than the critical density, the meniscus will appear to fall, going through the bottom of the cell at the temperature at which the gas density on the coexistence curve equals the average density in the cell. If the density is very close to the critical density, the compressibility of the fluid is large enough so that a density gradient is set up, and the meniscus will remain within the cell; the relative volumes as a function of temperature may then be used to provide a sensitive check of the density relative to the critical density.

The experimental check is made by slowly heating the sample cell in a water bath and observing the behavior of the meniscus. If the meniscus goes through the top or bottom of the cell the temperature at which the system becomes totally one phase is noted; density is determined from the coexistence curve for the material. Close to the critical density adjustments to density are made until the volumes of the two phases are equal just below the critical point. By this method one estimates that each of the samples is within $\frac{1}{2}\%$ of the critical density.

After filling and adjusting the density to the critical density, the sealed cell is removed from the gas system and weighed to determine the mass and average density of the sample. A sample calculation of the critical density for N_2O is given in Table 5. Table 6 compares the critical densities and temperatures observed in this experiment with other published results. Since the presence of small amounts of impurities can affect the critical densities as well as the critical temperatures for any given sample, the most accurate indication that a particular sample is at its critical density is the position of the meniscus at the center of the sample cell. The calculation of the density is useful mainly for comparison with other results. The densities measured in this experiment are consistent with previously determined critical densities.

Temperature Measurement and Control

The object of any experiment dealing with critical phenomena is to determine the behavior of the system as a function of the temperature difference from the critical point. To find this temperature difference

Table 5. Calculation of Critical Density for N₂O

Mass of cell with N ₂ O			1843.0 gms
			1843.0 gms
			1843.0 gms
Average			1843.0 ± 0.1 gms
Mass of empty cell			1818.4 ± 0.1 gms
Mass of N ₂ O	=	1843.0 - 1818.4	= 24.6 ± 0.2 gms
Density	=	$\frac{24.6 \pm 0.2}{53.3 \pm 0.8}$	= .460 ± 2.3% = .46 ± .01

Table 6. Critical Data for N₂O, CClF₃ and CH₃F

Investigators	T _c (°C)	P _c (Atm)	ρ _c ($\frac{\text{gm}}{\text{cm}^3}$)	n _i (ρ _c)
N ₂ O				
Villard ⁴⁴	38.8		.454	
Kuenan ⁴⁵	36.0	71.9		
Cardoso and Arni ⁴⁶	36.5	71.65		
Quinn and Wernimont ⁴⁷			.459	
Int. Crit. Tab. ⁴³	36.5	71.7	.45	
Cook ⁴⁸	36.34*	71.12	.452	
Straub ¹⁷	36.416*			1.1154
This Experiment	36.29		.468	
Albright and Martin ⁴⁹	28.85	38.2	.578	
Straub ¹⁷	28.715			1.0996
Schoenes ⁶	29.05			
This Experiment	28.33		.568	
Collie ⁵⁰	44.9	62.0		
Matheson Co. ⁴²	44.6	58		
This Experiment	44.26		.306	

*The value of the critical temperatures are not that reported in the original papers, but result from analysis of the data in reference (17)

one must know as precisely as possible the critical temperature of the system as well as the current temperature. In addition, the temperature of the system should be controlled for a time long enough for the system to reach an equilibrium state and to allow measurements characterizing the behavior at the temperature. These requirements for precise measurement and control in this experiment are met by placing the sample cell containing the fluid in a circulating bath, controlling the bath temperature with a proportional temperature controller, and measuring the temperature with a thermistor in a Wheatstone bridge.

The fluid bath consists of approximately 5 gallons of 2 centistoke viscosity Dow Corning 200 fluid in a 12" diameter, 12" high black anodized aluminum container surrounded by 1 to 3" of insulating foam except at those places in the sides of the cell where flat windows for optical paths are located.

Thermistor Bridge

The primary temperature measuring device for this experiment consists of a thermistor immersed in the fluid bath. A thermistor is used rather than a mercury in glass thermometer because the thermistor has greater sensitivity, it may more easily be used to produce a permanent record of the system temperature, and its behavior is more regular when measuring temperature changes of the order of a few hundredths of a degree. The thermistor was calibrated against a platinum resistance thermometer, so the temperature corresponding to a particular resistance is known. A temperature measurement is then made by measuring the resistance of the thermistor with the thermistor as one leg of a Wheatstone bridge. One of the sample cells also has a thermistor em-

beded directly in the cell. This has been used to check temperature variations between cell and bath.

Calibration Procedure

The thermistor is a thermally sensitive resistor with a large negative coefficient of resistance, of the order of 3% per^o C. The change in resistance between two temperatures is described by the following equation⁵¹

$$R(T) = R(T_0)e^{\theta \left(\frac{1}{T} - \frac{1}{T_0} \right)} \quad 3-2$$

$R(T)$, $R(T_0)$ are the resistances at the temperatures T and T_0 , θ is a constant of the individual thermistor. To calibrate the thermistor the temperature and resistance must be measured at two points and θ calculated for the interval between the two points.

Whenever there is power expended in a thermistor, the thermistor will be at a higher temperature than the surrounding medium. For this reason, the thermistor was calibrated under conditions that closely approximate the conditions under which the thermistor is used. It was calibrated in a water bath with respect to a platinum resistance thermometer (PRT) (Leeds and Northrup Model 8163-C). The thermistor resistance was measured in the Wheatstone bridge used in the experiment; the resistance of the PRT was measured using a Mueller bridge. The PRT had been calibrated by the Leeds and Northrup Co. with a calibration traceable to the National Bureau of Standards; the temperature scale used in that calibration was the International Practical Temperature Scale of 1948. The temperature corresponding to a particular resistance value of the

PRT was calculated using the Callendar formula:

$$T = 100 \frac{R_T - R_o}{R_{100} - R_o} + \delta \left(\frac{T}{100} - 1 \right) \frac{T}{100}$$

R_T = PRT resistance measured

R_o = PRT resistance at ice pt.

R_{100} = PRT resistance at steam pt.

$\delta = 1.492$ for this thermometer

Temperature and thermistor resistance values were calculated for several pairs of points and θ was calculated for a temperature and resistance range between each pair of points using the following equation obtained by solving Equation 3-2 for

$$\theta = \frac{T T_o}{T_o - T} \ln \left[\frac{R(T)}{R(T_o)} \right] \quad 3-3$$

Temperature Calculation

The temperature corresponding to a given resistance is calculated using the solution of Equation 3-2 for T

$$T = \left[\frac{1}{T_o} + \frac{1}{\theta} \left(\ln \frac{R(T)}{R(T_o)} \right) \right] \quad 3-4$$

T is the temperature to be calculated, R(T) is the resistance measured, R(T_o) is the resistance of one of the end points of the range within which R is measured. T_o is the temperature corresponding to R(T_o), θ

is that calculated for the particular range in which $R(T)$ is found. As a check of the sensitivity of the above equation to the value calculated for θ , a calculation for one endpoint of an interval was made using the other endpoint and a value of θ approximately .7% high. The error was approximately 15/1000 of a degree. This variation in θ is higher than the variation in θ between adjacent intervals, although a general increase in the value of θ is noted as T increases.

Uncertainties in Temperature Calibration

The uncertainty in the determination of temperature with the thermistor and Wheatstone bridge is due to uncertainties in the calibration of the thermistor against the PRT and in the calibration of the PRT against the standard temperature scale. The accuracy with which the thermistor could be calibrated against the PRT is limited by the accuracy with which the resistance of each could be measured. The thermistor resistance was measured during calibration to an accuracy of 0.05 ± 0.03 ohms; the resistance of the PRT was measured with a sensitivity of 10^{-4} ohms. This resistance sensitivity corresponds to a temperature sensitivity of 10^{-30} C for the PRT. The uncertainties for a particular calibration point are ± 0.03 ohms in resistance and 0.001° C in temperature. When two resistance-temperature points are used to calibrate a range on the thermistor, the uncertainty of the temperature at a point in the range will be due to the temperature and resistance uncertainty of the endpoints, as well as the uncertainty in the measured value of the resistance. The uncertainty in the resistance reading is approximately 0.03 ohms, corresponding to a temperature uncertainty of approximately 0.001° C in the temperature region of inter-

est. The uncertainty in the endpoints adds another 0.002° C uncertainty so the total uncertainty in the reading is 0.003° C.

In this experiment, the quantities of interest are temperature differences. For temperature differences in the same range, the calibration uncertainty is less, because the same endpoints and same θ are used to calculate both numbers. The calibration uncertainty is approximately

$$\text{Uncertainty} = \frac{\text{Difference in R values} \times 0.002^{\circ} \text{ C}}{\text{Range in R}}$$

For temperatures that are close to each other, the calibration uncertainty is negligible and the uncertainty is just the uncertainty due to the uncertainty in the two measured resistance values, approximately 0.002° C. For temperature differences between temperatures not in the same range, the uncertainty is the sum of the uncertainty in each value or 0.006° C. For N_2O , temperatures within 0.7° C of the critical point are within the same calibration range, and for CClF_3 and CH_3F temperatures within 1.5° C are in the same calibration range. The absolute uncertainties in the temperature measurement can not be accurately determined, because the calibration of the PRT does not give estimates on the probable errors in the calibration, but it is probably of the order of 0.01° C, the uncertainty in the determination of the International Practical Temperature Scale.

Temperature Control

Control of the temperature of the fluid inside the sample cell is achieved by controlling the temperature of the bath in which the cell

is immersed. This control is accomplished by decoupling the bath from changes in heat inflow or outflow and by using a proportional temperature controller to supply heat at a rate that equals the rate at which heat is lost from the system. The decoupling is accomplished by three methods:

(1) A synchronous motor powers the stirrer avoiding variations in heat input to the bath due to variations in line voltage.

(2) The temperature of the room in which the experiment is carried out is lowered so that changes in room temperature will have relatively less effect on the rate of heat outflow from the system.

(3) Relatively large amounts of insulation between the bath and room are used.

A Bayley model 252 proportional temperature control controls the bath temperature by means of a resistance heater along the inner walls of the bath. The heater is a 500 watt heater, but resistors are placed in series with the heater, but outside the bath, to reduce the effective heating power inside the bath to either 30 or 100 watts, depending on the temperature at which the bath is being controlled. This enables the controller to provide power at a rate between 20% and 80%, in which range it is most effective in maintaining control. The degree of control is largely determined by the stirring. Vigorous stirring is necessary to achieve good control, but with an ordinary propeller type stirrer, stirring adequate for temperature control produces bubbles which are unacceptable because the light beam passes through the fluid. This difficulty is avoided by the use of a flat disk approximately 3" in diameter which stirs the fluid without producing bubbles.

With the control operating normally, a rapid fluctuation of the temperature of approximately 0.001° C around the control temperature occurs. This fluctuation in bath temperature does not show up when checked with a thermistor imbedded inside a sample cell. On a short term basis for times of the order of 30 minutes, control to within $\pm 0.002^{\circ}$ C is achieved, for longer terms, depending on the temperature of the room, or the output from the air conditioning units in the room, the control is degraded to $\pm 0.004^{\circ}$ C for periods of 1 to 3 hours, and $\pm 0.008^{\circ}$ C for periods up to 12 hours.

This degradation of the control does not materially affect the results obtained because, in the temperature range greater than 0.1° C from the critical point, small deviations from the temperature control point show up immediately as a change in turbidity, and as the temperature returns to the control point, the turbidity returns to its original value. Although appreciable lengths of time are required for the system to reach equilibrium after large changes, the system mirrors small changes, of the order of 0.01° C very quickly. Thus an actual temperature sensitivity of a few millidegrees is possible and meaningful.

Measurements with an Optical Bridge

The actual turbidity of the fluid as a function of temperature is measured by means of an optical bridge. The use of an optical bridge enables accurate measurements of the intensity transmitted through the sample cell to be made by comparing it to the intensity of a reference beam which can be adjusted by attenuation. The intensity

of the cell beam relative to the reference beam is then determined by measuring the amount of attenuation necessary to produce equal intensities. Although absolute intensity measurements cannot be made, intensity readings may be made with an empty cell and a filled cell and with filled cells at different temperatures and the relative intensities compared.

The variable attenuator consists of three Glan Thompson (GT) polarizing prisms arranged so that there is one rotatable prism in a divided circle rotator between the two fixed prisms in the optical path. The two fixed GT prisms are aligned with the same direction of polarization, so the light intensity transmitted through the three prisms is proportional to $\sin^4 \theta$, where θ is the angle between the direction of polarization for the center prism and the direction for which the transmission is a minimum.

The polarizers are aligned by placing the first GT prism in the optical path and aligning it to give some convenient direction of polarization. The rotatable prism is then placed behind the first prism and rotated until minimum transmission is obtained.

The third prism is then put into place and rotated until a new minimum of transmission is found. This aligns the first and third prisms so that they have the same direction of polarization. This method is used since relative changes in intensity are much greater near transmission minima than near maxima. The $\sin^4 \theta$ dependence was checked by means of neutral density filters and found to hold within the error limitations of the neutral density filters.

Optical Bridge Components

The various components of the optical bridge are shown in schematic form in Figure 7. The light source for the bridge is a Spectra Physics Model 133 laser which emits unpolarized light at 633 nm. The output is well collimated, having a divergence of approximately 1 mrad., with a beam diameter at the sample cell of about 2 mm.

The beam first passes through a red filter removing any blue light from the plasma tube and then through the first GT prism (placed before a beamsplitter so that both beams will be polarized). The beamsplitter separates the beam through the sample cell from the reference beam. The reference beam then passes through the second and third prisms of the attenuator, the oil bath, and a lens which focuses the beam onto the plane of a chopper. The other beam passes through the bath, the sample cell, a circular aperture 3.0 mm in diameter, and another lens which focuses this beam in the plane of the chopper. The chopper is aligned so that the two beams fall alternately on the face of an RCA 7265 photomultiplier (PM) tube which is used to measure the intensity of the light. A diffusing screen is mounted in front of the PM tube to minimize the effects of beams incident at different positions on the tube. The tube is powered by a Keithley Model 240 power supply; where the turbidity is small, the supply voltage is -1500 volts. Close to the critical temperature, the transmitted light intensity decreases as the turbidity increases and the supply voltage is increased. This voltage was chosen for the greatest sensitivity on the devices used to measure the output from the tube. The voltage due to the photocurrent (approximately .03 ma) through a 10^4 ohm resistor is displayed on a

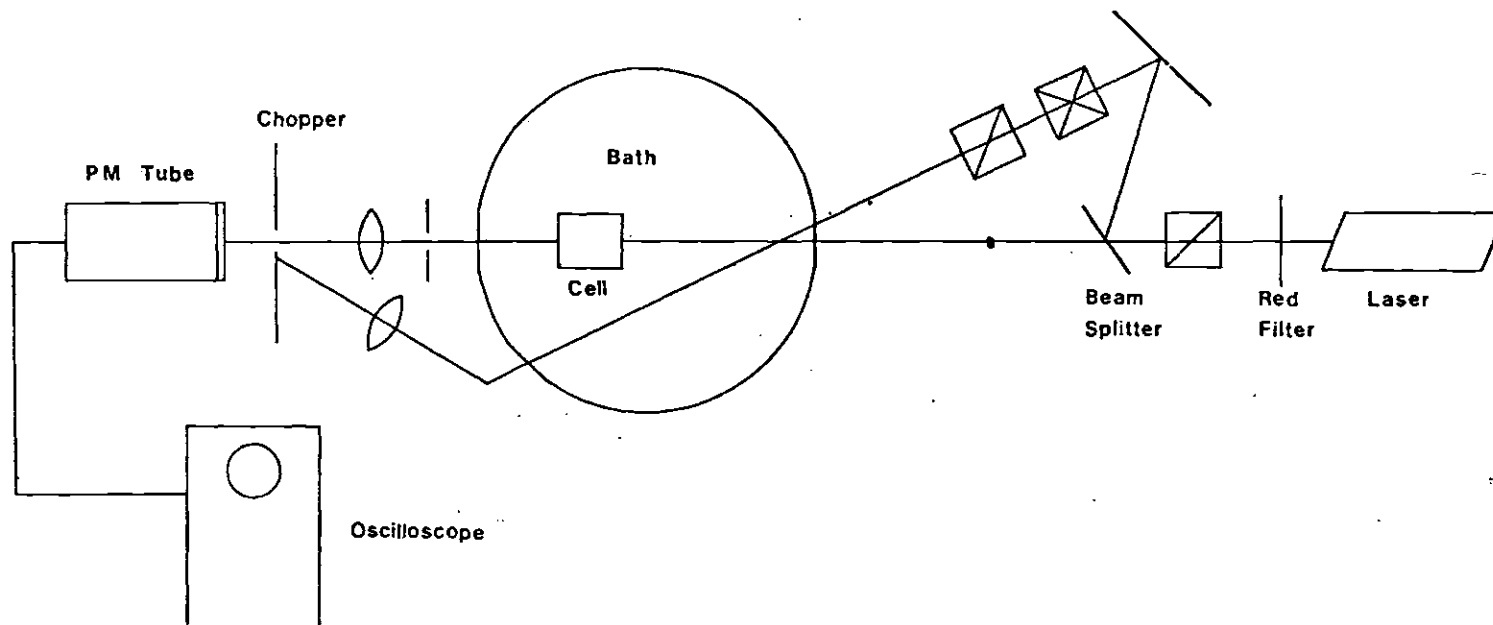


Figure 7. Optical Bridge Components

Model 535 Tektronix oscilloscope.

Since the beams have been focused at the plane of the chopper, the rise time during which the intensity of the beam transmitted by the chopper changes is much less than the time during which there is full transmission or full extinction, and the output from the photomultiplier tube due to each beam has the form of a square wave. Because of the size of the slits on the chopper, the transmission time for each beam is less than the blocking time. Since the beams fall alternately on the face of the PM tube, the resulting signal consists of two alternating square waves with the amplitude of each proportional to the incident light.

The circular aperture in the beam that passes through the sample cell serves two purposes: first, it limits the amount of forward scattered light reaching the PM tube; second, it eliminates possible effects due to multiply scattered light. It is movable so that variations in beam position (such as that produced by a downward bending of the beam due to density gradients in the sample near the critical point) may be matched. With this aperture in place, the errors in the measured light intensity due to inclusion of the forward scattered light may be determined from the scattering equations presented in Chapter II. The half acceptance angle of this aperture is approximately 6×10^{-3} rad. At 0.026° C above the critical temperature, the smallest ΔT used in the final analysis of the correlation lengths, the forward scattered light represents only 0.03% of the measured light intensity; farther away, the error is less. The maximum possible error due to multiple scattering may be determined by assuming that all of the light scattered

out of the beam is then scattered a second time and estimating the amount of this multiply scattered light that passes through the aperture. Calculations show that the maximum error due to this multiple scattering is approximately the same as the error due to the inclusion of the forward scattered light. Since not all of the light is multiply scattered, the error will be less than this maximum calculated; the error will become still smaller for larger ΔT .

Positioning of Sample Cell

The sample cell is positioned so that the beam traverses the cell horizontally at the point where the meniscus disappears as the temperature is raised past the critical temperature. This accurate vertical positioning is necessary because the very large compressibility of a fluid near its critical point results in large density gradients in the fluid. Only a small region at the center of the cell will actually be at the critical density, and it is at this point in the center of the cell that the meniscus disappears as the temperature is raised. These density gradients close to the critical temperature also bend the light beam downward. This effect, however, is only important for temperatures very near the critical point. Deviations of the beam were not noted in this experiment until the temperature was less than 0.2° C above the critical temperature. The time required for these density gradients to become established increases greatly for temperatures near the critical point, and since no equilibrium data was obtained closer than 0.1° C from the critical temperature, density gradients did not pose a serious problem for this series of experiments.

The power of the beam through the sample should be reduced to a

point where no heating of the sample occurs due to heating by the beam. The beam power through the sample in this experiment is less than 50 microwatts. Swinney and Cummins³⁵ found that beam powers less than 75 microwatts did not affect similar samples of CO₂, so heating is not considered to be a problem for this series of experiments.

Data Acquisition Procedures

A measurement of the light intensity transmitted through the sample cell is made by rotating the center GT prism until the intensities of the two beams are equal, as determined from the oscilloscope trace. Since the output from the PM tube consists of two alternating square waves, the oscilloscope is adjusted so that the trace is triggered by each pulse; there is a stable display of two pulses, one from each beam, superimposed on the screen. The center GT prism is rotated until the flat portions of each pulse coincide. The amplitude of the signal from each beam is the same, and thus the intensities of the two beams are equal. The angle of the rotatable prism is recorded, and the process is repeated for a total of four readings. The readings are averaged, and the difference between this average angle and the angle for minimum transmission is calculated. The intensity may then be determined from the $\sin^4 \theta$ law.

The angles of the rotatable GT prism may be measured to the nearest 0.05°, with the minimum detectable intensity variation corresponding to a change in the angular reading of approximately 0.05°. The percent error in measured intensity depends on the relative transmission, but for the intensities when the turbidity is small, the error is approximately 0.1%.

The optical system is very sensitive to slight movement of the optical components so absolute stability of the system is required during any data taking run. This is achieved by attaching all components firmly to rails which are then bolted to the table. The system is also sensitive to shifts in the beam position. The sample cell beam is steady, except for the density gradient bending, but the reference beam enters and exits the bath through non-parallel windows. Consequently, changes in the refractive index of the bath fluid with temperature cause shifts in the reference beam position. To take account of this effect, a series of readings were taken measuring the light transmitted through the cell with an empty cell in place of the filled cell over the temperature region of interest. Thus a baseline intensity was obtained for the transmission of an empty cell as a function of temperature.

The transmission of an empty cell is different from that of a filled cell because of the differing index of refraction of the material in the cell. At the inner surfaces of the windows, the light beam passes from a medium having one index of refraction to one with another index of refraction. For normal incidence the transmission at the interface is given by the formula⁵²

$$T = \frac{4 \frac{n_1}{n_2}}{\left[\left(\frac{n_1}{n_2} \right) + 1 \right]^2}$$

n_1 is the refractive index of medium 1;

n_2 is the refractive index for medium 2;

T is the transmission

The index of refraction for the air in the empty cell is assumed to be 1.000 while the indexes of refraction for N_2O and $CClF_3$ at the critical density have been measured and are given in Table 6. The refractive index for CH_3F at the critical density has not been measured, but for standard conditions of temperature and pressure, the index of refraction is given in the ICT⁴³ as 1.000449. Using the measured critical density and applying the Lorentz-Lorenz relation,

$$\frac{n^2 - 1}{n^2 + 2} = \frac{4\pi}{3} \alpha \rho$$

n = refractive index

α = polarizability

ρ = density

an index of refraction of 1.0904 may be calculated for CH_3F at the critical density.

Using the known index of refraction for quartz, and the values of the refractive index for the various materials in the cell, the transmission may be calculated for each surface for both the empty cell and the filled cells. This value is then squared to obtain the total transmission for the interior surfaces. The appropriate corrections to the baseline for the empty cell may be made for each of the filled cells to obtain a value for the transmission through each fluid in the absence of scattering from the fluid within the cells. When light

intensity measurements are made with the cells containing the fluids, the measured intensity should be less than the adjusted baseline close to the critical point and approximately equal to the adjusted baseline for temperatures 10° C or more away from the critical temperature. The difference then would be due to the light scattered from the fluid inside the cell, from which the turbidity as a function of temperature for the fluid could be determined. In some cases, this is not exactly correct. The quartz windows have imperfections which may affect the transmission; there may be a small difference of position of the cells in the bath; and the indexes of refraction for the N_2O and $CClF_3$ have been determined using the sodium D line, $\lambda = 589$ nm, while the laser light used is of a different frequency, $\lambda = 633$ nm. In addition, the index of refraction for the CH_3F has not been accurately determined and the effect on the light transmission of the polymer coating on the interior of the cell windows in the cell containing CH_3F is not known.

Experimentally, these differences result in the observed intensities lying above or below the adjusted baseline. If the intensities lie above the baseline, a log-log plot of the positive turbidities vs temperature difference from the critical point will have a downward curvature for $\Delta T > 0.2^{\circ}$ C. If the intensities lie below the baseline, then a log-log plot as before will show an upward curvature with the turbidities approaching a constant value. The correct baseline will result in a straight line when the turbidity is plotted vs ΔT . So the final choice of the correct baseline may be made by choosing that baseline which gives the straightest line for $\Delta T > 0.2^{\circ}$ C. This is done mathematically rather than graphically by varying the baseline to mini-

mize the error when the turbidity is fitted to a function of the form of Equation 2-42:

$$\tau = C\Gamma e^{-\gamma}.$$

CHAPTER IV

DATA AND ANALYSIS

Data Analysis Procedure

The first step in the data analysis for each of the substances investigated is the determination of the critical temperature of the substance. The criterion for the transition is the appearance of a meniscus and the beginning of nucleation marking the separation into two phases; the critical temperatures measured in this way are given in Table 6. The turbidity at a temperature is determined from Equation 2-38 in which the incident intensity is the measured baseline, adjusted for the difference in transmission at the windows of the filled cell, and the transmitted intensity is just the measured intensity with the filled cell in place. ΔT is determined by subtracting the measured critical temperature from the temperature at which the turbidity is determined, and turbidity τ vs ΔT data is obtained. This data is plotted for the various substances in Figure 8 on page 84, Figure 10 on page 90, and Figure 12 on page 96.

This turbidity vs ΔT data is fit to an equation of the form 2-41 using a generalized least squares fitting program, LSQG. This program, shown in Appendix C, is an element in the physics program library file, PH*LIB. LSQG calculates a best least squares fit to functions of the form

$$\sum_{n=1}^N a_n f_n(\vec{x}_i, \vec{C}) \quad 4-1$$

where the a 's are parameters to be fitted. Equation 2-42 is written in the form of Equation 4-1 using logarithmic functions, resulting in two parameters, one the logarithm of the coefficient and the other the exponent. The best fit parameters a_1 and a_2 are those for which the variance is minimized; the uncertainty in the determination of the a 's is given by the standard deviation of the fit. The program LSQG itself handles the input of data, calls on a subroutine to evaluate the functions, converts the data into matrices, uses another subroutine to invert the matrices, and finally calculates the parameters and associated errors.

The graph of the turbidity vs ΔT should be a straight line in the temperature range in which the correlation length is negligible; but close to the critical temperature, as the correlation length increases, the exponent describing the slope should become smaller (in absolute value) as the curve flattens out. It is desired to use temperatures as close to the critical temperature as possible in calculating the exponent while keeping only that portion of the curve that is a straight line. To do this, various minimum values of ΔT are used to fit the turbidity- ΔT data, and the minimum ΔT used is that smallest ΔT for which there is no consistent decrease in γ . Points as close to the critical temperature as 0.2°C are used for all of the fluids investigated. For points closer to the critical temperature than $\Delta T = 0.2^\circ \text{C}$, there is a constant decrease in the exponent attributable to the effects of the increasing correlation length.

The magnitude of the constant C in Equation 2-40 is calculated

using the measured index of refraction at the critical density, the measured critical density and critical temperature, and the constants λ_0 and k . C is then used to determine the coefficient of the compressibility. The value for the compressibility is then used to calculate the correlation lengths for each fluid for values of $\Delta T < 0.2^\circ \text{C}$.

Possible uncertainties in the intensity measurements result in an uncertainty of approximately 0.0005 cm^{-1} in the turbidity measurement. In addition, there are other errors that lead to larger uncertainty in the turbidity data. The first of these is due to possible changes in the position of the beam transmitted through the sample cell or errors in the transmission function calculated for the window surfaces. Such errors result in a consistent shift of the entire baseline and may be treated as described in Chapter III. Other errors, due to changes in the reference beam position, result in inconsistencies between various portions of the measured turbidity- ΔT curve. The magnitude of such errors is not known precisely, but judging from the experimental data, may result in differences amounting to $\pm 0.0002 \text{ cm}^{-1}$. The effects of this type of error may be eliminated by fitting the data points to Equation 2-42 with no weighting for all $\Delta T \geq 0.2^\circ \text{C}$. The LSQG program calculates an error in the determined critical exponent; the range of the data is reduced by taking successively smaller maximum ΔT and the error is determined for each range and plotted against the maximum ΔT . In each case, the error is relatively large for the entire range considered, but as the maximum ΔT becomes less, there is a rapid decrease in the error until some minimum error is found; a further de-

crease in the range results in a slight increase in the error due to the small number of data points considered. The decrease in the magnitude of the error is accompanied by a change in the calculated critical exponent. This change in exponent becomes less as the change in the error decreases, and the exponent finally reaches, in all cases, an approximate final value for the same maximum ΔT at which the error is minimized. This indicates that the data in the range for which the errors are approximately constant is self-consistent. This is expected because the range over which the data is self-consistent represents only a small temperature change and thus a small possible change in the reference beam position.

The turbidity values in this self-consistent range may then be adjusted as described in Chapter III to determine whether the curve might best be fit with some adjusted baseline. There was no indication that adjustments to the baseline improved the fit for either of the three substances investigated.

In addition, the errors determined for the isothermal compressibility may be checked by attempting to use values of the compressibility outside of the error bounds to calculate the correlation lengths. This was done for the N_2O and resulted in confirmation that values outside of the error bounds result in incorrect values for the correlation lengths, either too large or too small, relative to the observed total light scattered.

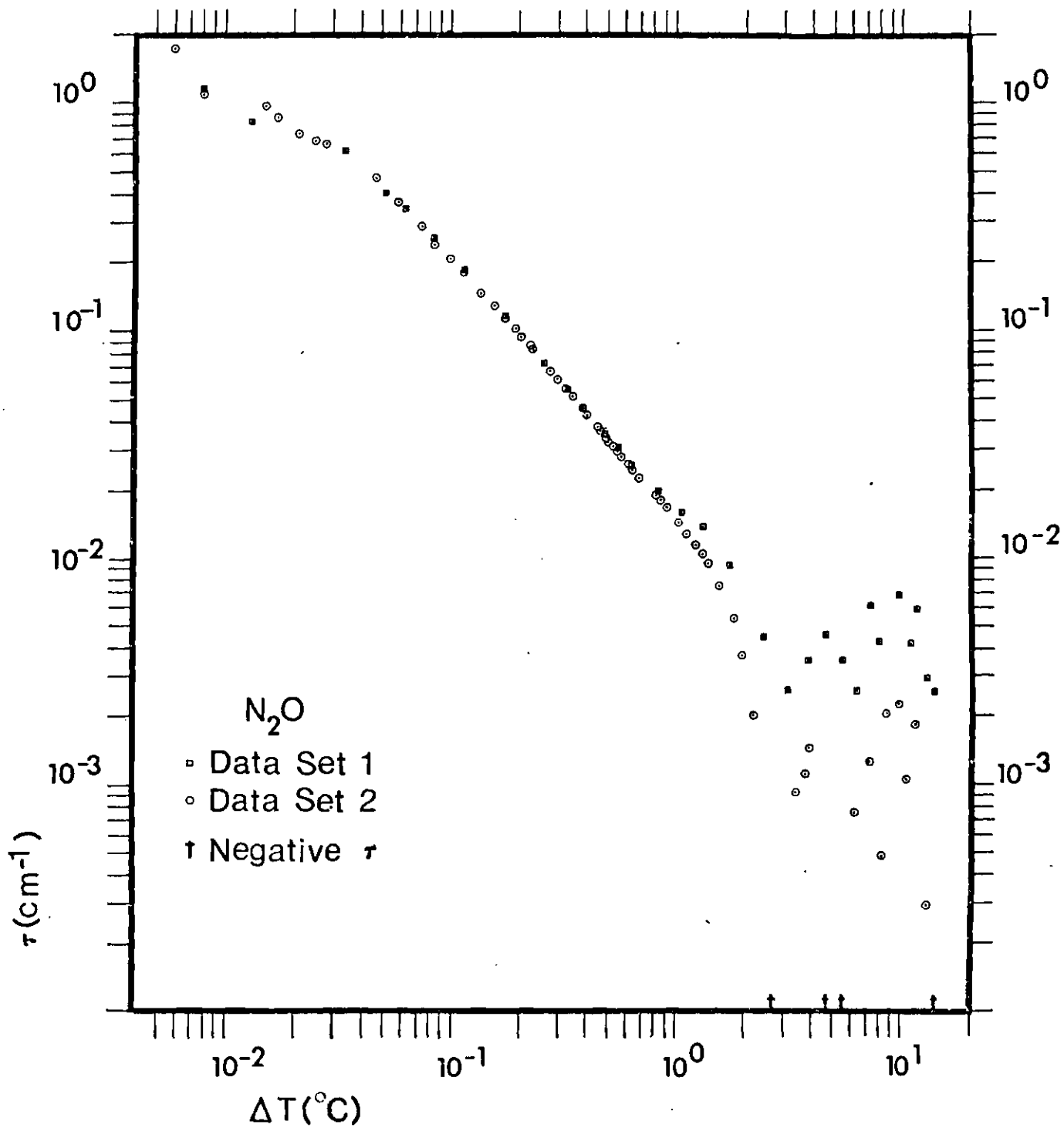
Determination of κ_T

Data Analysis for N_2O

Two sets of turbidity vs ΔT data, shown in Figure 8, are used in the analysis of the N_2O data. The same baseline is used in both cases, but the relative transmission of the optical components is different in each case, accounting for the difference in the two data sets. The data sets are analyzed separately and together; the results of these analyses are in agreement and are consistent with the accuracy expected from the experiment, as well as with the errors calculated in fitting the data.

N_2O Data Set 1. Critical exponents and errors calculated for this data set for various ranges of temperature are plotted in Figure 9. The data from $0.2^\circ C$ to $2^\circ C$ from the critical temperature is apparently self-consistent, judging from the approximate constant error for smaller ranges and the rapidly increasing error outside this range. There is, however, a steady and significant increase in the calculated exponent within this range as the maximum ΔT is reduced, increasing from $\gamma = 1.07$ to $\gamma = 1.16$ for the smallest range considered. Considering the data without any adjustments, it is reasonable to expect that the data closest to the critical point, which has the smallest relative error, would give the best determination of γ . This may be checked by adjusting the data in the range $0.2 < \Delta T < 2.0$ for best fit. When this is done, a value for γ

$$\gamma = 1.175 \pm .011$$

Figure 8. Turbidity vs. ΔT Data for N_2O

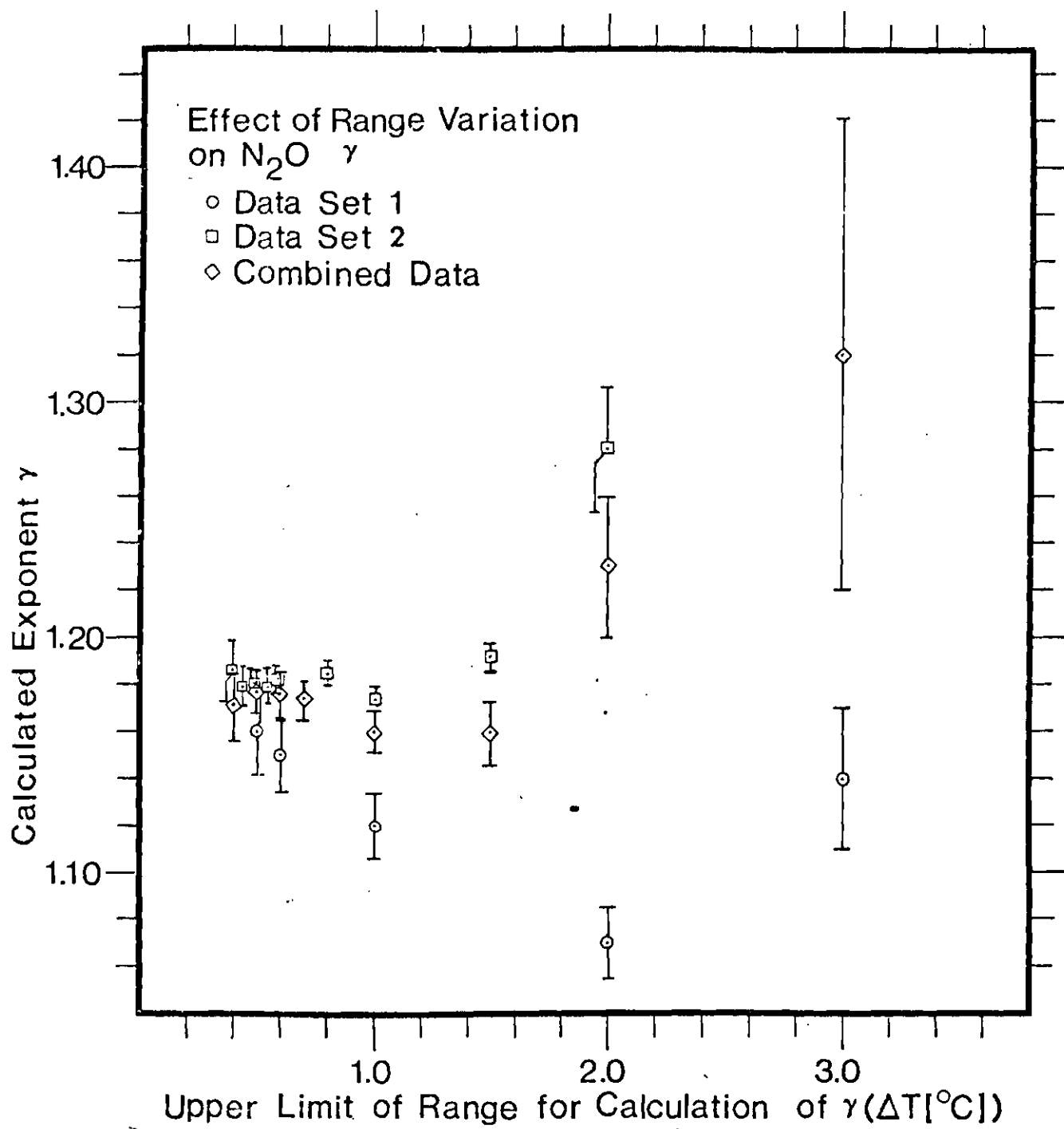


Figure 9. Effect of Range Variation on N_2O γ

is calculated. A range with a slightly higher minimum ΔT gives a value $\gamma = 1.16 \pm .02$; a slightly smaller range results in $\gamma = 1.19 \pm 0.013$. The smaller ranges have larger errors than the total range $0.2 < \Delta T < 2.0$, as expected, because the greater range should give a better fit due to the larger number of points. The adjustments required for each range, however, are of about the same amount, approximately -0.002 cm^{-1} ; consequently, the best fit value for the complete range is considered to be the best value. The values for γ found by the analysis of the first N_2O data set, then, are

$$\begin{array}{ll} \gamma = 1.16 \pm .02 & \text{unadjusted near } T_c \\ \gamma = 1.175 \pm .011 & \text{adjusted best fit value} \end{array}$$

N_2O Data Set 2. The second data set used in the analysis of the turbidity- ΔT data for the N_2O consists of a considerably larger number of data points than the first set, resulting in smaller errors. The turbidity values measured for this set appear to be slightly smaller than the corresponding values measured for the first set, indicating that some different correction might be needed; and this is the case.

The data for this second set is checked by varying the range as in the first data set with the results shown in Figure 9. The data appears to be self-consistent for the range $0.2 < \Delta T < 1.5$, with the values close to the critical temperature best fit with $\gamma = 1.180 \pm .006$, for which the error is smallest. Considering the entire range for which the data is considered to be self-consistent, a best fit is obtained with the addition of approximately 0.0008 cm^{-1} to the measured

values of the turbidity, resulting in a value for γ of $1.160 \pm .005$, a value slightly smaller than that obtained by considering only values of ΔT close to the critical temperature. So the two values determined are

$$\begin{array}{ll} \gamma = 1.180 \pm .006 & \text{unadjusted near } T_c \\ \gamma = 1.160 \pm .005 & \text{adjusted best fit value} \end{array}$$

The numbers are not in perfect agreement, considering the errors calculated, but the difference is small.

N₂O Data--Both Sets. A similar check of the effects of range variation with the combined data from both sets is also plotted in Figure 9. This check yields a minimum error with the range $0.2 < \Delta T < 0.6^\circ \text{C}$ and a corresponding value for γ ,

$$\gamma = 1.176 \pm .008$$

No significant decrease in the error is found by varying the measured values of turbidity.

Because this exponent value is determined using data from both sets, it is considered to be the most accurately determined; in addition, the value lies between the values calculated for each of the separate data sets. Consequently, this value is taken as the value for γ for the N₂O. The range of values calculated, however, indicates that the error bounds should be extended to include the value at $\gamma = 1.16$, and so the actual error in the determination is ± 0.015 . In addition, the uncertainty in the determination of the critical temper-

ature leads to a further uncertainty in the exponent of approximately 0.01. The total uncertainty in the exponent, then, is ± 0.025 and the best value calculated for γ for the N_2O is

$$\gamma = 1.176 \pm .025 .$$

The fitting of the data that produced the above value of the exponent produces a value of $(0.01455 \pm 0.0006) \text{ cm}^{-1}$ for the turbidity coefficient, and so the turbidity may be written

$$\tau = (.0146 \pm .0006) \Delta T^{-\gamma} (\text{cm}^{-1}); \gamma = 1.176 \pm .025 .$$

Compressibility Calculation from Turbidity. On the basis of the measured critical index of refraction and the measured critical density, the Lorentz-Lorenz formula may be used to calculate the $\left(\frac{\partial \epsilon}{\partial \rho}\right)$ for the N_2O . The quantity C from Equation 2-38 may then be calculated, and the coefficient describing the compressibility then determined from the measured values of turbidity and the calculated C. This introduces approximately another 2% error into the coefficient calculation, although not into the calculation for the exponent.

The measured values are:

$$\rho = .46 \text{ g/cm}^3$$

$$\frac{\partial \epsilon}{\partial \rho} = .574 \text{ cm}^3/\text{g}$$

$$\lambda_o = 633 \text{ nm}$$

$$kT_c = 4.28 \times 10^{-4} \text{ ergs}$$

from which C may be determined;

$$C = \frac{8}{3} \pi \left(\frac{\partial \epsilon}{\partial \rho} \right)^2 \frac{\pi^2}{\lambda_0^4} kT_c = 151.6 \times 10^{-4} \text{ atm/cm}$$

The coefficient describing the behavior of the isothermal compressibility as a function of ΔT is then

$$(.959 \pm .07) \text{ atm}^{-1}$$

κ_T expressed as a function of ΔT may be written

$$\kappa_T = (.96 \pm .07) \Delta T^{-\gamma} \text{atm}^{-1}; \gamma = 1.176 \pm .025 \quad 4-2$$

or, expressed in terms of the reduced temperature,

$$\kappa_T = (1.14 \pm .07) 10^{-3} \epsilon^{-\gamma} \text{atm}^{-1}; \gamma = 1.176 \pm .025 \quad 4-3$$

This value of the compressibility, together with the unadjusted measured values for turbidity is then used to calculate the correlation length for the N_2O as a function of temperature.

Data Analysis for $CClF_3$

The turbidity- ΔT data for $CClF_3$ is shown in Figure 10; the results of the analysis by means of a variation in the range similar to that detailed earlier for N_2O are shown in Figure 11. This analysis indicates that the data is consistent for the range $0.2 < \Delta T < 1.0$, since for this range and for all smaller ranges the fitted value for γ

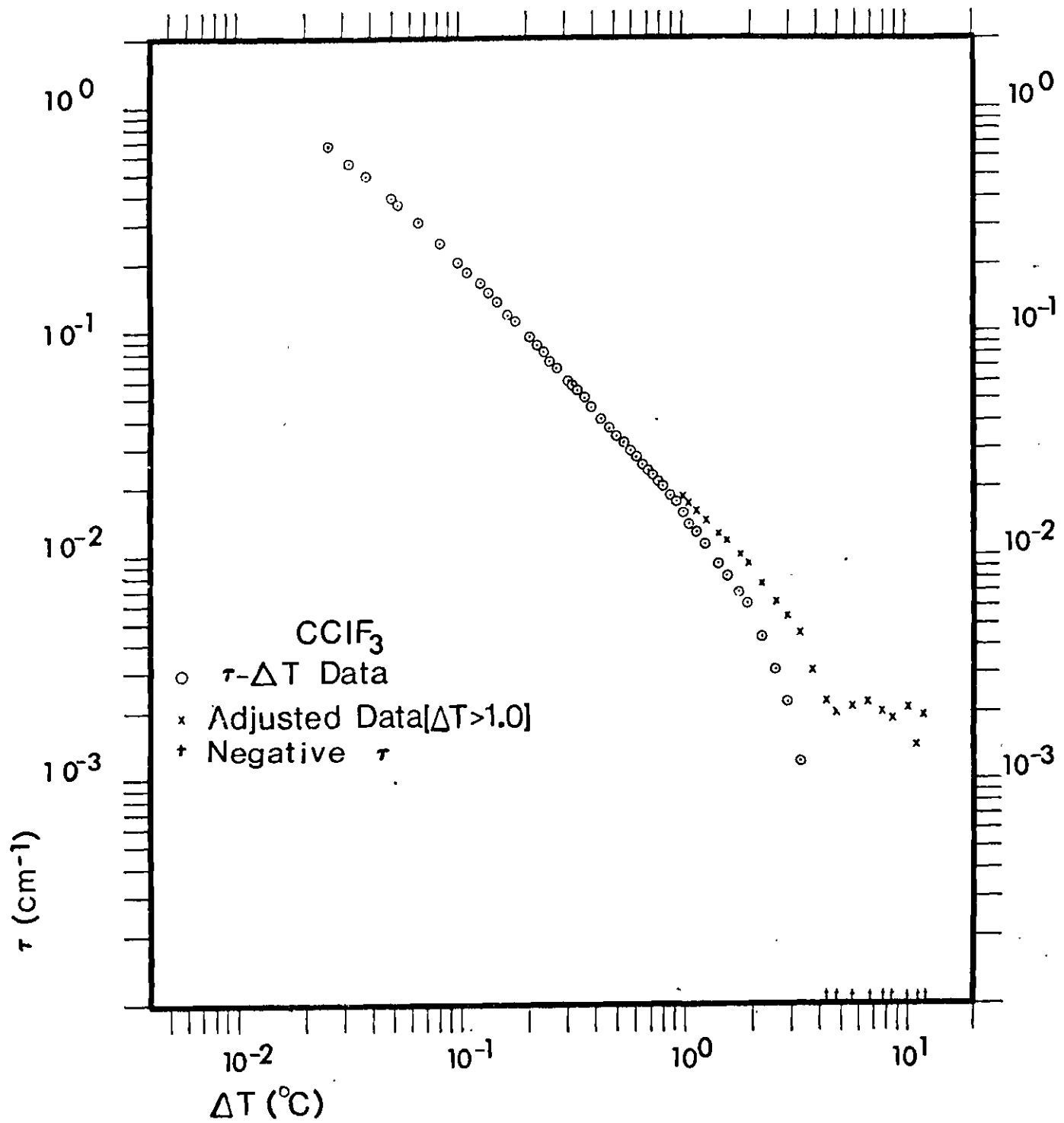


Figure 10. Turbidity vs ΔT Data for CClF3

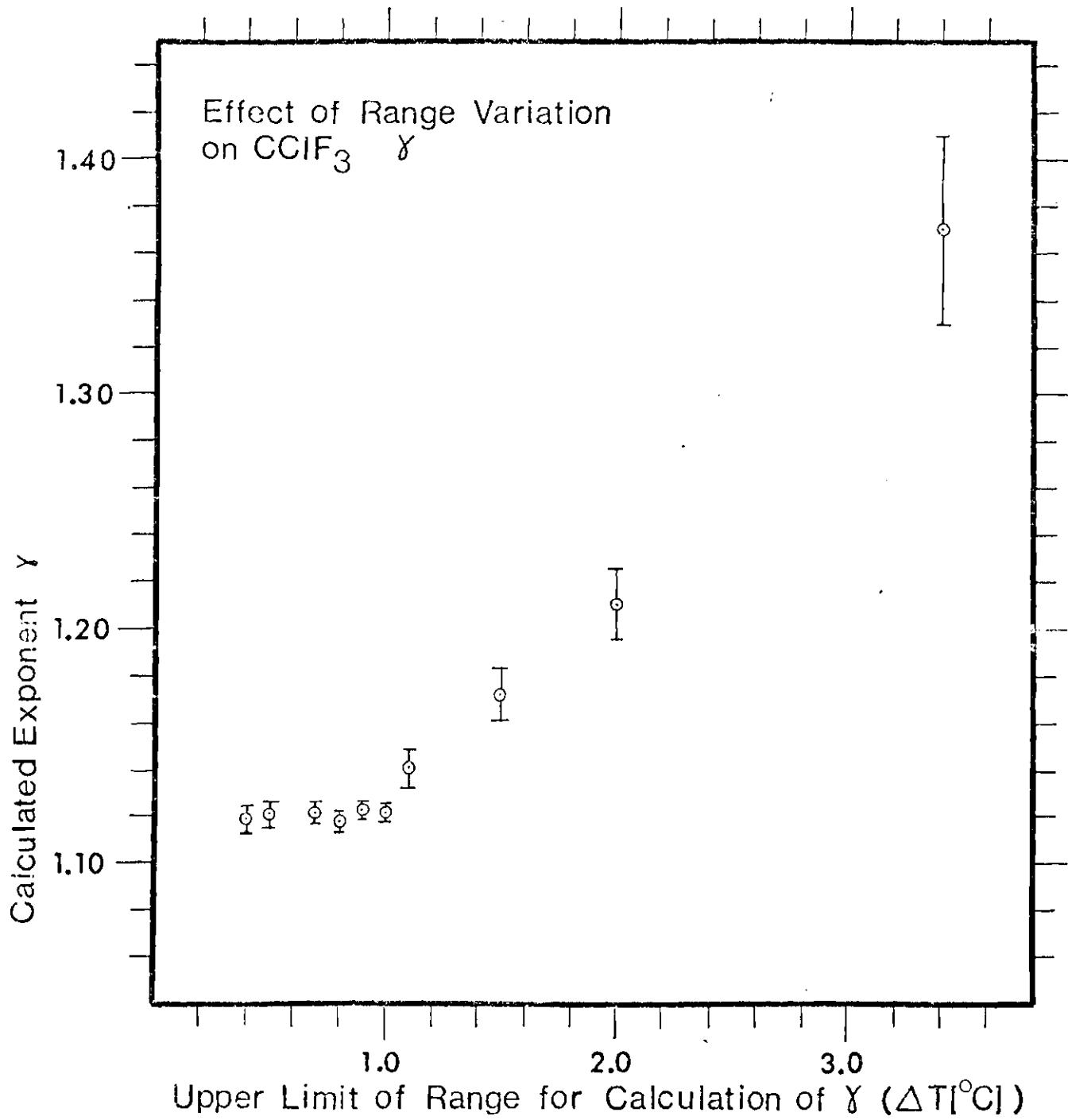


Figure 11. Effect of Range Variation on CClF_3

is approximately the same and the errors approximately constant, while there are rapidly increasing errors outside this range. The value and error for γ calculated on this basis are $\gamma = 1.120 \pm 0.003$. When the turbidity values in the range for which the data is self-consistent are adjusted in order to obtain a best fit, the best fit is found to be given by the unadjusted baseline with γ the same value as above. In addition the slope and thus the exponent were the same for all of the smaller ranges considered. It was found, however, that a shift in the exponent by ± 0.005 had no significant effect on the error; the actual uncertainty then is the sum of the above errors, ± 0.008 . The values calculated for γ then are the same:

$$\begin{array}{ll} \gamma = 1.120 \pm .003 & \text{unadjusted baseline} \\ \gamma = 1.120 \pm .008 & \text{best fit} \end{array}$$

Comparison of the range variation data with Figure 10 indicates that at the point where the data becomes inconsistent, there is an abrupt change in the slope of the line. The possibility that this change in slope is due to a change in the exponent attributable to the dipole-dipole interaction has been investigated, but the effect has been found to be due to experimental inconsistencies between various portions of the data. First, an effect due to the dipole-dipole interaction should result in a value for γ close to 1.0, and the value 1.12 is relatively far from 1.0. Second, analysis of the data for $\Delta T > 1.0^\circ \text{C}$ indicates that the curve can be fit with an exponent in the range 1.1 - 1.6 (but with considerably larger errors than for $\Delta T < 1.0^\circ \text{C}$) with the addition

of approximately 0.0028 cm^{-1} to the measured values for the turbidity, shown by the x's in Figure 10. The large difference in the adjustment needed for the two portions indicates that there is an experimental inconsistency between the two portions of the data curve. Third, attempts have been made to fit the entire curve with one adjustment over the entire temperature range investigated. When this is done, however, the calculated value of γ shows a significant increase as the critical temperature is approached, a behavior contrary to that expected on the basis of a dipole-dipole interaction. In addition, as will be seen in the next section, there is no similar effect observed with the CH_3F . Since the dipole moment of the CH_3F is some three times the size of the dipole moment of CClF_3 , the absence of such an effect in the CH_3F confirms that the change in slope is not due to the effects of the dipole-dipole interaction.

Compressibility Calculations from Turbidity. With the above fitted value for the exponent, the turbidity for CClF_3 as a function of ΔT is best fit by the expression

$$\tau = (1.633 \pm .010) \times 10^{-2} \Delta T^{-\gamma} (\text{cm}^{-1}) \quad \gamma = 1.120 \pm .018$$

The errors are considered to be the larger of the two errors calculated earlier. The constant C is calculated as for the N_2O , with an error of approximately 2% as before. For the CClF_3

$$n_c = 1.0996$$

$$\rho_c = .57 \text{ g/cm}^3$$

$$\frac{\partial \epsilon}{\partial \rho} = .392 \text{ cm}^3/\text{gm}$$

and

$$C = \frac{8}{3} \pi \left(\rho \frac{\partial \epsilon}{\partial \rho} \right)^2 \frac{\pi^2}{\lambda_o^4} kT_c = 106.4 \times 10^{-4} \text{ atm/cm} .$$

Analyzing as for the N_2O , the formula for κ_T is

$$\kappa_T = (1.54 \pm .04) \Delta T^{-\gamma} \text{ atm}^{-1}; \gamma = 1.120 \pm .025 \quad 4-4$$

Expressed in terms of the reduced temperature this becomes

$$\kappa_T = (2.57 \pm .07) \times 10^{-3} \epsilon^{-\gamma} \text{ atm}^{-1}; \gamma = 1.120 \pm .025 \quad 4-5$$

Data Analysis for CH_3F

The data analysis procedure for the CH_3F is the same as for the other fluids investigated. The transmission of the filled cell in the absence of scattering is calculated as described in Chapter II from the measured baseline, but since the baseline is measured using uncoated windows and the CH_3F cell windows are coated with the silicone polymer, the calculation for the difference in transmission between filled and empty cell must take the polymer coating into account. This is done, and turbidity- ΔT data for the CH_3F is shown in Figure 12 with the results of range variation shown in Figure 13. Although the errors calculated for the CH_3F are considerably larger than those for the other two fluids, the data appears self-consistent for the range $.2^\circ C < \Delta T$

$< .6^{\circ}$ C. The error is smallest for the range $.2^{\circ}$ C $< \Delta T < .55^{\circ}$ C for which range the value of the exponent γ calculated is $\gamma = 1.154 \pm 0.024$. There is a slight apparent increase as the range is further decreased, but this is accompanied by an increase in the error. If the points in the range for which the error is least are weighted proportional to the turbidity, the calculated value of the exponent is increased to $\gamma = 1.16$ with no significant change in the error. When attempts are made to adjust the turbidity to give a best fit, there is a general decrease in the error with the addition of some constant value to the measured values of turbidity. For the range in which the error is smallest, weighted values of the turbidity give a best fit of $\gamma = 1.11$ while the non-weighted data shows no significant changes on adjustment. Other ranges likewise show no significant changes, tending to contradict the indications of a slight increase in the slope as the range is decreased; in addition, checks made by calculating the correlation lengths for various values of γ indicate that the errors are slightly less with the lower value of γ . In the absence of consistent indications that the value of γ should be higher or lower than the measured value for which the error is least, this measured value is taken as the actual value of γ for CH_3F . Error bounds of ± 0.05 should be large enough to reflect the uncertainty in the actual measurement; including, for example, the value $\gamma = 1.11$. When the uncertainty in the exponent due to the uncertainty in the determination of the critical temperature is added, the actual value of γ , with errors, is

$$\gamma = 1.15 \pm .06$$

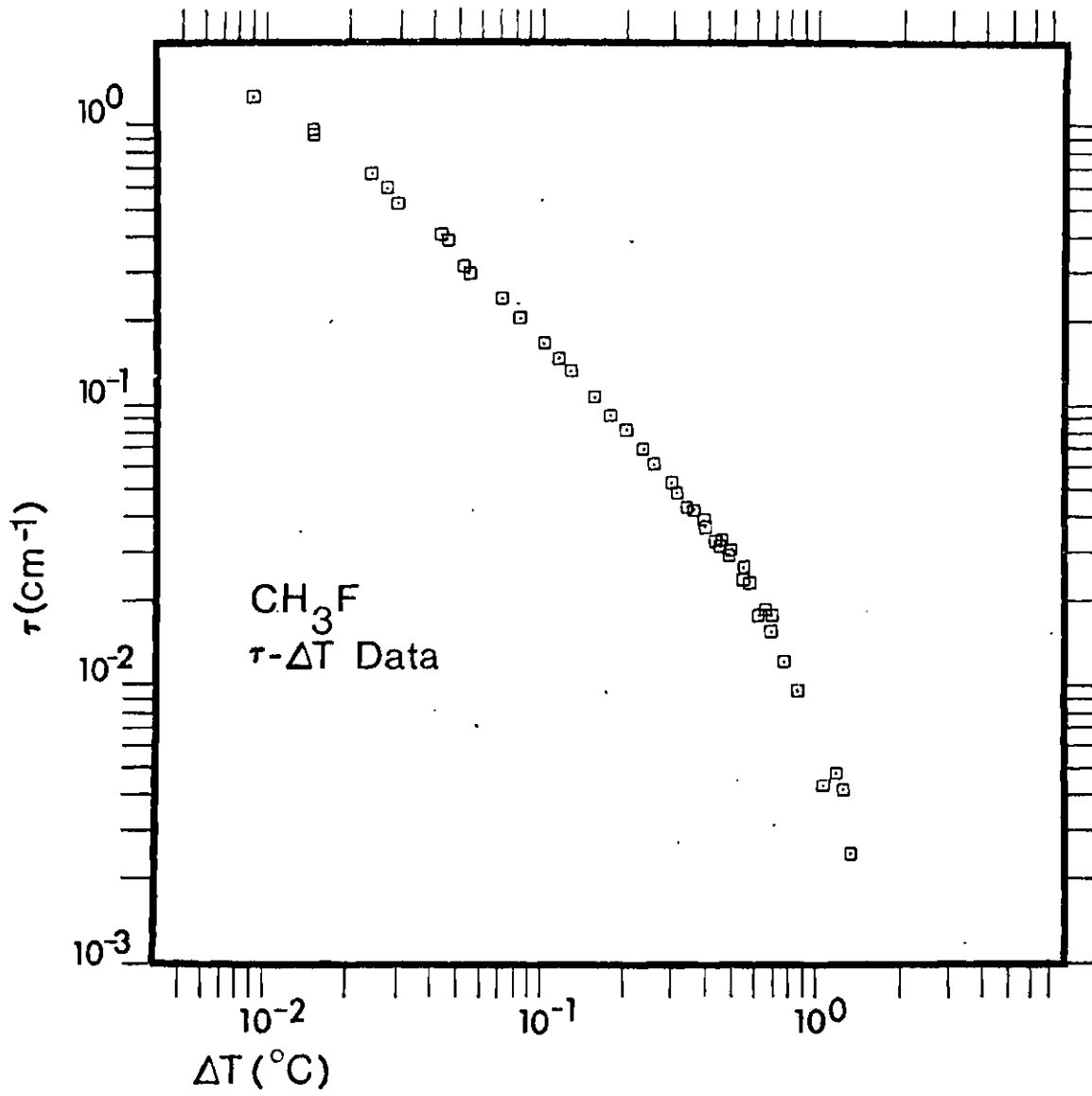


Figure 12. Turbidity vs ΔT Data for CH_3F

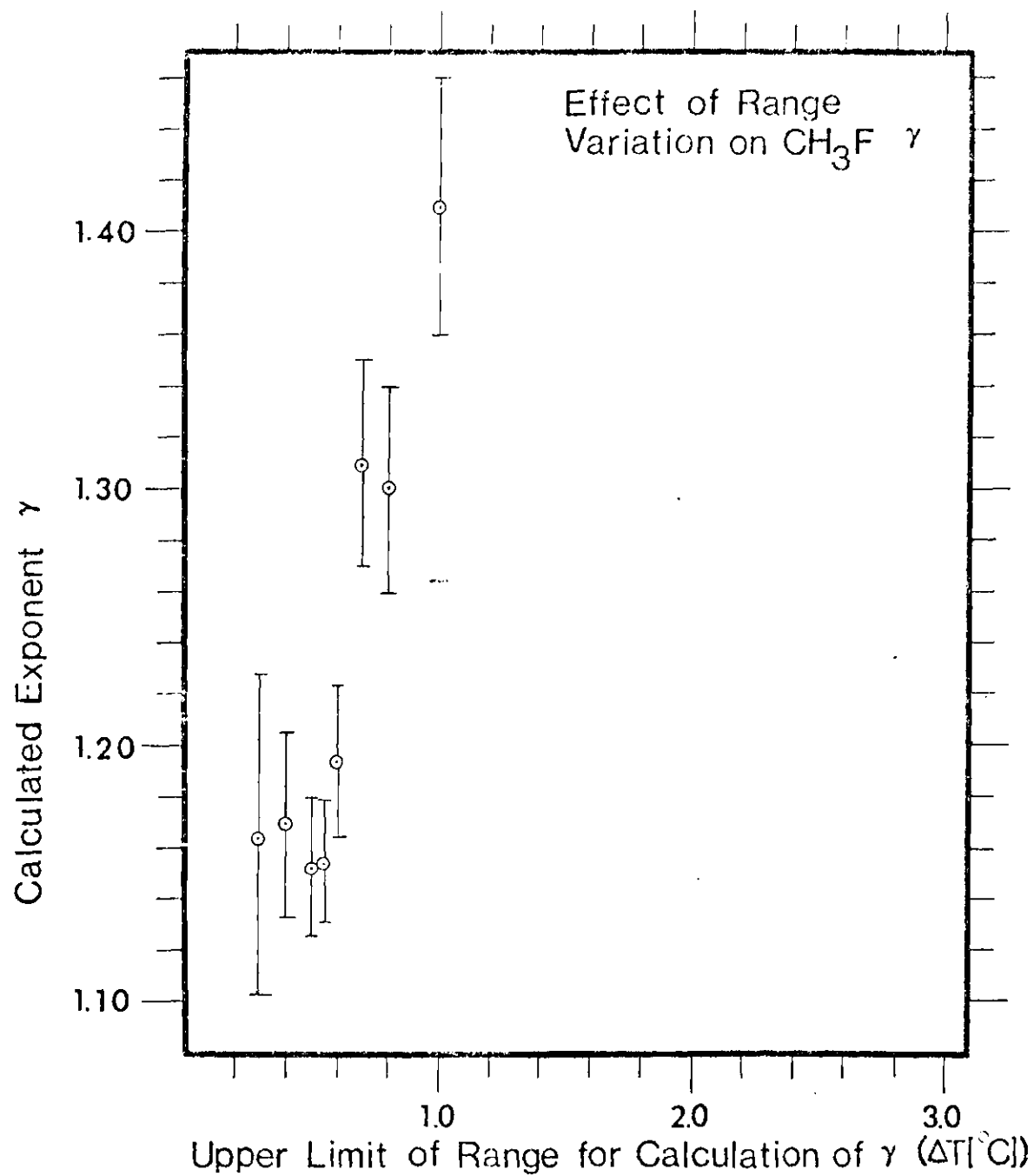


Figure 13. Effect of Range Variation on CH_3F

Compressibility Calculation from Turbidity. Considering the uncertainties in the fitting of the CH_3F data, the turbidity is given by

$$\tau = (.0130 \pm .0015) \Delta T^{-\gamma}$$

$$\gamma = 1.15 \pm .06$$

For CH_3F

$$n_c = 1.0904$$

$$\rho_c = .306$$

$$\frac{\partial \epsilon}{\partial \rho} = .6564$$

and

$$C = \left(\frac{8}{3\pi}\right) \left(\frac{\partial \epsilon}{\partial \rho}\right)^2 \frac{\pi^2}{\lambda_o^4} kT_c = 89.6 \times 10^{-4} \text{ atm/cm} .$$

The compressibility as a function of ΔT is

$$\kappa_T = (1.45 \pm .16) \Delta T^{-\gamma} \text{ atm}^{-1}; \gamma = 1.15 \pm .06 \quad 4-6$$

which when expressed as a function of the reduced temperature is

$$\kappa_T = (1.92 \pm .20) \times 10^{-3} \epsilon^{-\gamma} \text{ atm}^{-1}; \gamma = 1.15 \pm .06. \quad 4-7$$

Experimental Determination of ξ_o and ν

Correlation lengths are calculated for the fluids investigated in this series of experiments following the procedures discussed in

Chapter II; the results are shown in Figure 14. These values of ξ vs ΔT are then fit to an equation of the form

$$\xi = \xi_0 \Delta T^{-\nu}$$

using the LSQG program detailed earlier for various ranges of $\Delta T \leq .2$ C for the combined data for all substances and for the N_2O , $CClF_3$, and CH_3F data separately. There is considerable scatter in the data leading to relatively large errors in the calculation of the fitting parameters describing the behavior of the correlation length; these uncertainties are due to the fact that two relatively large numbers, each with associated errors, are subtracted, resulting in a small number with relatively large error. Considering only the uncertainties in the measurement of the light intensities leads to an uncertainty in the measured correlation lengths of $\pm 200 \text{ \AA}$. Possible uncertainties in the fitting of the compressibility lead to additional uncertainties in the measured fit for the ξ - ΔT data.

Figure 14 indicates, however, that there are no major differences in the measured correlation lengths for the three fluids. In particular, there is no indication from the graph that the differing dipole moments of these three fluids have any effect on the measured correlation lengths. This is confirmed by analysis that shows that the uncertainties involved in fitting the data for each substance are larger than the differences calculated for the various fluids.

Combined Data for Three Fluids

The combined correlation length- ΔT data for the N_2O , $CClF_3$, and

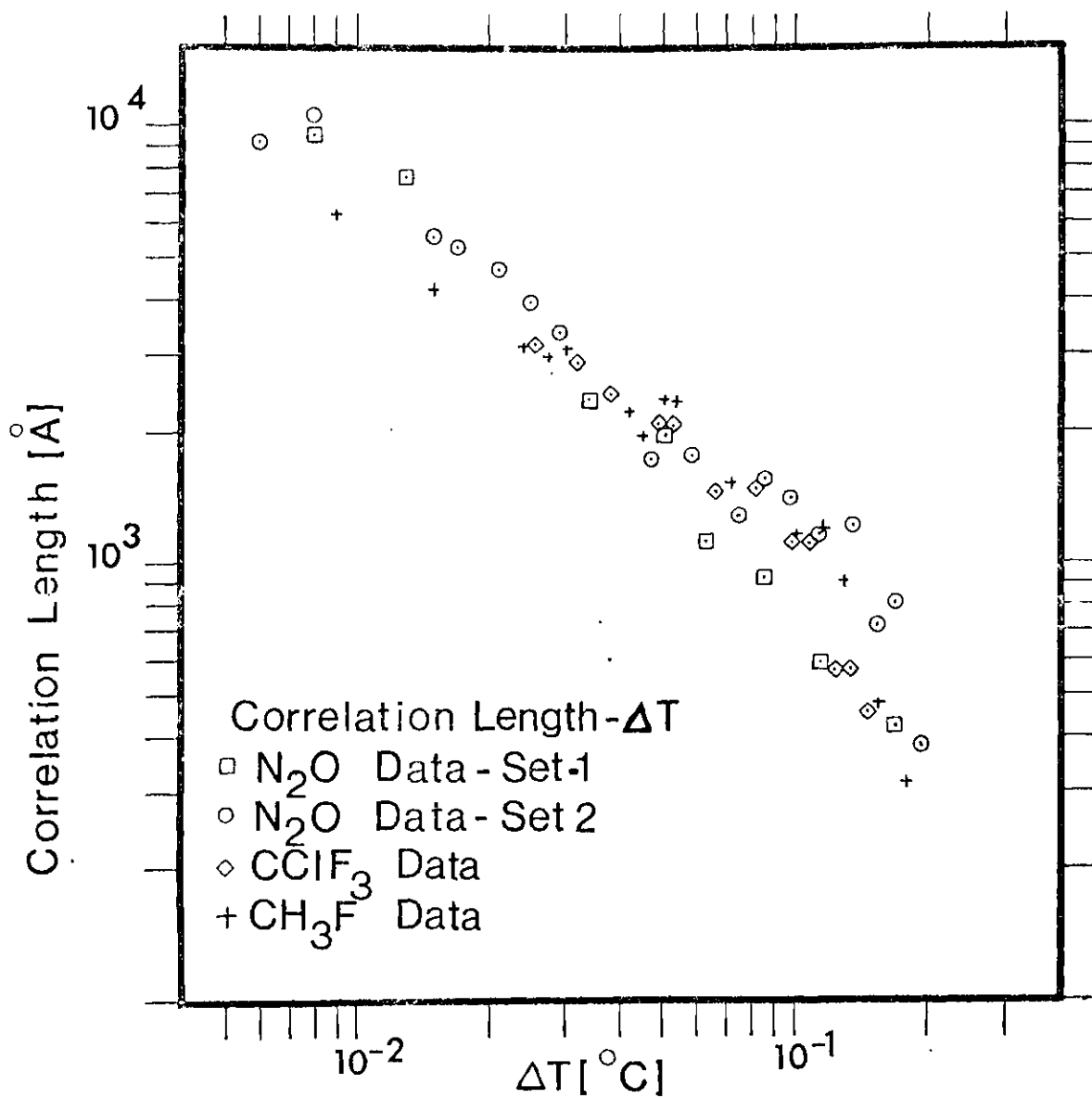


Figure 14. Correlation Length vs T Data for N₂O, CClF₃, CH₃F

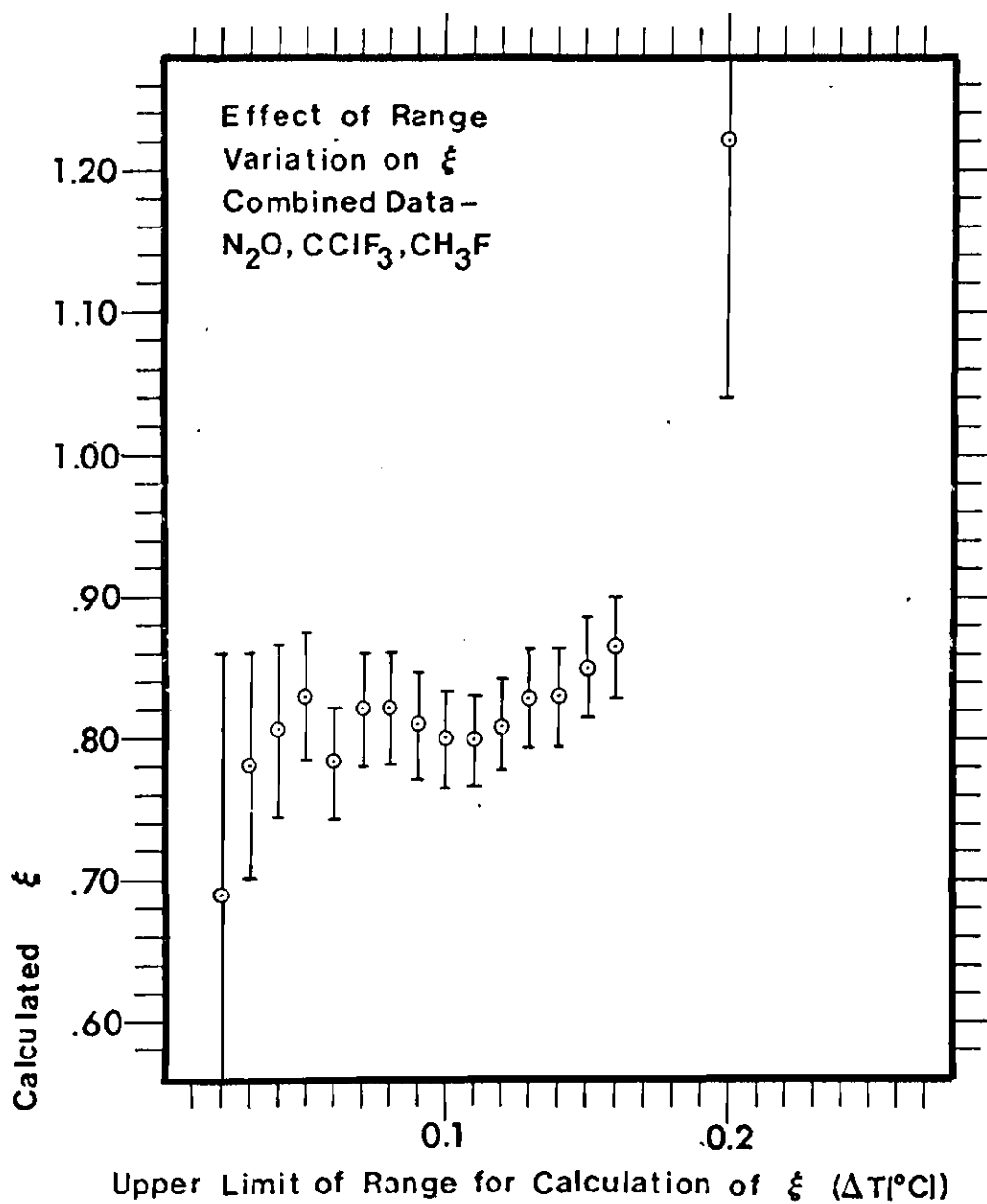


Figure 15. Effect of Range Variation
on ξ for $N_2O, CClF_3, CH_3F$

CH_3F is fitted with the LSQG program for $.006^\circ \text{C} \leq \Delta T \leq 0.2^\circ \text{C}$ and for various ranges having a smaller maximum ΔT ; the results are plotted in Figure 15. There is a large decrease in the error and in the calculated exponent when the maximum ΔT is reduced from .20 to .16, and only a slight change in the error for smaller ranges; consequently the range $\Delta T \leq .16^\circ \text{C}$ is taken as the range in which the data appears self-consistent. The minimum error occurs for the range with maximum $\Delta T \leq 0.11$, and for this range, the correlation length- ΔT data appears best fit by

$$\xi = (180 \pm 20) \Delta T^{-\nu} \text{ \AA}$$

$$\nu = (.80 \pm .03) \quad 4-8$$

The fit for various ranges indicates that there is a general decrease in the measured exponent ν as the range is decreased by choosing the maximum ΔT closer to the critical point. This decrease in ν is accompanied by an increase in the coefficient. Calculation of fitting parameters for the substances separately shows that this same general behavior occurs, so comparison of the exponents and coefficients for various substances should be made using the same range of data in each case.

Comparison of ξ_0 , ν for N_2O , CClF_3 , CH_3F

CClF_3 has the largest minimum ΔT and thus the smallest range measured, so the range determined for CClF_3 will determine the ranges used for the other substances. Variation of the CClF_3 range as for the above combined data indicates that there is a large decrease in the error and change in ν for the range $\Delta T \leq 0.11$; so this range is taken as the self-consistent range for the CClF_3 . Fitting parameters are then

calculated using the range $0.025 \leq \Delta T \leq 0.11$ in each case. The results are shown below:

Combined data-all substances

$$\xi = (200 \pm 40) \Delta T^{-(.76 \pm .07)} \quad 4-9$$

CClF_3

$$\xi = (200 \pm 25) \Delta T^{-(.77 \pm .04)} \quad 4-10$$

CH_3F

$$\xi = (250 \pm 70) \Delta T^{-(.70 \pm .09)} \quad 4-11$$

N_2O -both sets

$$\xi = (125 \overset{+ 50}{- 40}) \Delta T^{-(.90 \pm .13)} \quad 4-12$$

The values calculated for ν are consistent when error bounds are taken into account, but the ν for N_2O is slightly greater than for the other two substances. This discrepancy is removed when the two sets of N_2O data are analyzed separately. Analysis shows:

N_2O -Data Set 1

$$\xi = (48 \overset{+ 20}{- 14}) \Delta T^{-(1.17 \pm .13)} \quad 4-13$$

N_2O -Data Set 2

$$\xi = (215 \overset{+ 60}{- 45}) \Delta T^{-(.75 \pm .08)} \quad 4-14$$

ξ and ν calculated for Data Set 2 are in very close agreement with the other values calculated; the N_2O data set 1 differs from the other set and from the other substances considered by a considerably larger

amount. This difference is probably due to the fitting procedure used, in which both sets are used in determining the best fit parameters for K_T . Since there are considerably more data points in set 2 than in set 1, the fitting parameters are primarily determined by data set 2. Slight differences in the sets, in particular a difference in the calculated coefficient, account for the differences in the calculated ν . Since the fitting is determined primarily by data set 2, it is thought that data set 2 offers the best comparison with the other substances, in which case there is no longer a significant difference between the N_2O data and that of the other substances.

The only remaining difference is in the CH_3F data, and this difference in exponent is less than the error calculated. As a further check, the ν is calculated for $\gamma = 1.11$, a number that differs from the best value of γ by approximately the error bound calculated for the CH_3F γ . When this is done, the ν calculated is $\nu = 0.62 \pm 0.09$. So evidently the uncertainty in the determination of γ accounts for an uncertainty in ν of approximately ± 0.08 in addition to the errors calculated on the basis of the standard deviation. So the total uncertainty is considerably larger than the difference between the CH_3F and the other substances, leading to the conclusion that the difference is not significant.

General Discussion of Correlation Length Measurements

Comparison of Equations 4-9, 4-10, 4-11, and 4-12 indicates that when the range is held constant, there are no significant differences in correlation length parameters calculated for the three fluids investi-

gated. The values of ξ_0 and ν are, however, larger than values reported for other substances^{20,53}. Limitation of data to ranges close to the critical point tends to result in lower values of ν with larger coefficients, and with larger errors on each; extending the range to larger ΔT results in lower values for the coefficient with larger values of ν , together with much larger errors. In addition, when turbidity values for $\Delta T > 0.2^\circ\text{C}$ are included, the uncertainties in the measurement of the turbidity result in some measured values of turbidity being slightly larger than that calculated on the basis of the best fit parameters for the compressibility. This results in negative values for α in Equation 2-32, causing a breakdown in the calculation of the correlation length.

Because of the changes in the parameters calculated for various ranges, and because of discrepancies between this data and other reported values for the correlation length, it is thought that there are possible systematic errors in the data close to the critical point; but the data for each substance is taken using the same procedures, and any differences between the various substances are expected to result in differences in the calculated fitting parameters for these substances. There are no significant differences between the substances, with the slight differences that exist considerably smaller than the uncertainty in the fitting of the individual substances.

Discussion of Compressibility Results and Comparison with Other Experiments

The experimental measurements of Γ and γ describing the behavior of K_T in the critical region for the three fluids investigated in this

series of experiments are given in Equations 4-3, 4-5, and 4-7. These values are also given in Table 7, together with other determinations of critical exponents for N_2O , $CClF_3$ and CO_2 .

These measurements of κ_T in the critical region are the first reported for N_2O and CH_3F . Although there are no reported measurements for N_2O , this molecule is similar to CO_2 in its physical properties: the shape is the same, the molecular weight is the same, the critical parameters ρ_c , T_c , P_c are similar, and the one critical exponent that has been measured for both, β , is the same. The small dipole moment of N_2O would be expected to have either a small or no effect on the measured critical exponents, and so comparison of N_2O data of this experiment with other CO_2 data can be made. κ_T for CO_2 in the critical region has been measured using light scattering techniques by Lunacek and Cannell²⁰ and by White and Maccabe⁷. Their measured values are (in terms of the units used in this series of experiments):

Lunacek and Cannell

$$\kappa_T = (.785 \pm .047) \times 10^{-3} \text{ e}^{-\gamma}$$

$$\gamma = 1.219 \pm .01 \text{ atm}^{-1}$$

White and Maccabe

$$\kappa_T = (.986 \pm .08) \times 10^{-3} \text{ e}^{-\gamma}$$

$$\gamma = 1.17 \pm .02 \text{ atm}^{-1}$$

These values differ by more than the error reported for each experiment. However, the data of White and Maccabe seems better than

Table 7. $\kappa_T(\Gamma, \gamma)$, β , α for N_2O ,
 CO_2 , $CClF_3$ and CH_3F .

	$\kappa_T(\text{atm}^{-1})$ Γ	γ	β	α
This experiment	1.14×10^{-3}	1.176		.13*
<u>CO_2</u>				
Straub ¹⁷			.345	
Lunacek & Cannell ²⁰	$.785 \times 10^{-3}$	1.219		.09*
White & Maccabe ⁷	$.986 \times 10^{-3}$	1.17		.13*
Lipa et. al. ¹⁹				.12
<u>$CClF_3$</u>				
Straub ¹⁷			.354	
This experiment	2.56×10^{-3}	1.12		.17
Schoenes ⁶	$.764 \times 10^{-3}$	1.275		.017*
<u>CH_3F</u>				
This experiment	1.92×10^{-3}	1.15		

*Value for α predicted from experimental measurement of γ , Straub's measurement of β , and scaling laws.

that of Lunacek and Cannell in terms of the amount of data considered, the greater range of data (by approximately two decades) and correction terms considered. As seen in Table 7, the value for κ_T for N_2O is in excellent agreement with that of White and McCabe and in approximate agreement with that of Lunacek and Cannell. The coefficient for the compressibility for the N_2O is slightly larger than that for CO_2 , indicating a possibly greater correlation range for a given ΔT .

There has been one other measurement of κ_T for $CClF_3$, that of Schoenes⁶. There is serious disagreement between this experimental measurement and that of Schoenes who reports a value of

$$\kappa_T = (.764 \pm .05) \times 10^{-3} \epsilon^{-\gamma}$$

$$\gamma = 1.275 \pm .04$$

The reason for this lack of agreement is not known. The data of this experiment is generally consistent with measurements of Straub, who measured β for N_2O and $CClF_3$ and found that β for the $CClF_3$ is slightly closer to the classical value, but by an amount approximately equal to the error in the experiment. There is a greater relative change in this data for γ than in Straub's data for β .

No other experimental measurements have been made on CH_3F in the critical region, but in terms of the size of the coefficient the CH_3F data from this experiment is consistent with the data for $CClF_3$ from this experiment.

Comparison of Three Fluids

The exponents calculated for the $CClF_3$ and the CH_3F are somewhat

lower than that calculated for the N_2O . $CClF_3$ is apparently significantly lower (although when errors of both are considered, the error bounds do not exclude approximate equality), while the CH_3F is only slightly lower, with an uncertainty that includes the values of γ measured for each of the other substances.

Predictions from Scaling Laws

The scaling law $\alpha + 2\beta + \gamma = 2$, together with the measured values for β and γ may be used to predict values for the specific heat exponent α for $CClF_3$ and N_2O , neither of which has been measured. The values should be:

$$N_2O: \quad \alpha = .13$$

$$CClF_3: \quad \alpha = .17$$

These values, and α 's predicted on the basis of other experiments, as well as an experimental value for α for CO_2 are also shown in Table 7.

This value predicted for N_2O is consistent with the prediction of the Ising model ($\alpha = .125$) and the experimental value for CO_2 ($\alpha = .12$)¹⁹. The α predicted for $CClF_3$ on the basis of this experiment is slightly higher than that predicted for N_2O ; the value predicted on the basis of Schoenes's data is considerably lower.

Conclusions

γ and ν have been measured for three fluids, N_2O , $CClF_3$, and CH_3F , with the γ and ν data for N_2O and CH_3F the first reported for these substances. The data for γ for N_2O is in excellent agreement

with that for CO_2 as expected, but there is disagreement with a reported measurement for CClF_3 . While the data does not exclude the possibility that γ is approximately the same for all substances, there are indications that there are differences among the molecules.

Comparison with other non-fluid systems near their critical points indicates that the effect of a dipole-dipole long range interaction is the changing of the critical exponents from those that are characteristic of Ising-like systems to those characteristic of classical systems with long range forces. If dipole effects are very strong, as in ferroelectric systems, the exponents have classical values throughout the critical region. For systems in which the long range force is much weaker, as in ferromagnetic systems with magnetic dipole interactions, the critical behavior is primarily determined by the short range forces; but for temperatures very close to the critical temperature, the long range force may be expected to cause a change in the exponent from an Ising-like value to one closer to the classical value.

For the fluids investigated, CClF_3 has the smallest value for γ (closest to the classical value) while N_2O is close to values measured for non-polar fluids, and CH_3F has some intermediate value. This amount of deviation from the measured values for non-polar substances is not what would be expected if the effect were due to a dipole-dipole interaction; since the CH_3F is much more highly polar (by a factor of three) than the CClF_3 , an effect due to a dipolar interaction would be expected to be much more important for the CH_3F . But this is not the case, leading to the conclusion that there is no evidence that the di-

pole moment has any effect on the measured values of γ .

Consideration of correlation length data indicates that, although the data is not consistent with other reported values, there is general agreement in the correlation lengths and exponents calculated for the three fluids. The exponent calculated for CH_3F , the most polar, is slightly lower (nearer the classical value) than the others, but the difference is considerably less than the uncertainty in the fitting of the CH_3F data and is not considered to be significant. Since the correlation length data analyzed extends to $\Delta T = 0.026^\circ \text{C}$, and no significant variations attributable to the dipole-dipole interaction have been observed, the conclusion is that within the range of data considered ($\Delta T > 0.026^\circ \text{C}$, $\epsilon > 9 \times 10^{-5}$) the dipole interaction does not affect the measured critical exponents.

There does, however, appear to be a slight variation in γ ; and this variation is consistent with differences in the shapes of the molecules. N_2O is a linear molecule having the same shape as CO_2 ; these two fluids also have the same measured value for γ . CClF_3 , with an apparent lower value for γ , is a molecule with C_{3v} symmetry and approximately tetrahedral shape. CH_3F has a similar shape, but the atoms off the symmetry axis are hydrogen atoms rather than fluorine atoms. Since in terms of mass distribution the CH_3F molecule is intermediate between the CClF_3 molecule and the N_2O molecule, an exponent measurement intermediate between those for N_2O and CClF_3 would be consistent with an effect due to the molecular shapes. There is indication that this is the case, but the errors associated with the various measure-

ments do not allow this conclusion unequivocally. Further work on more complex molecules with different internal degrees of freedom and different symmetries to determine whether these do have a real effect on the measured exponents for fluids seems warranted.

Turbidity measurements are a useful way of measuring the critical behavior of fluids. Conceptually, they are extremely simple, but great care must be taken to avoid changes in intensity due to causes other than the changes in the fluid inside the cell. Two major improvements would be the avoidance of having a light beam passing through the oil bath that provides temperature control and the mounting of the complete optical system so that any one part is immovable with respect to the complete system, avoiding problems due to possible misalignment of components. The use of an Argon ion laser would provide greater scattering efficiency due to the $1/\lambda_0^4$ dependence of the scattering. This would increase the total amount of light scattered out of the beam, increasing the measured turbidity for a given ΔT and reducing the relative errors.

APPENDIX A

CALCULATION OF STRESS ON FUSED QUARTZ WINDOWS

The maximum stress on any circular plate, uniformly loaded, supported uniformly around the edges is given by the following formula

$$\text{stress} = \frac{3}{8} \frac{WR^2}{t^2} (1 + m)$$

m is Poisson's ratio, which for quartz is .16. W is the pressure in psi; R is the radius of the unsupported area, and t is the thickness of the plate. The units of stress are psi. For the quartz windows used in this experiment R is $\frac{1}{2}$ " and the working pressure is 1,200 psi, so the above equation may be written

$$\text{stress} = \frac{356}{t^2}$$

For a thickness of $\frac{1}{4}$ " the maximum stress is approximately 5,700 psi in the ideal case. Because of possible irregularities in the supporting shoulder or in the epoxy with which the window is attached the actual stress may be higher, possibly by 50% or more, so in any design a safety factor must be taken into account. The ultimate tensile strength of the quartz is 7,000 psi⁵⁴; thus there is danger of failure if windows of this thickness are used. This indeed occurred. For $\frac{1}{2}$ " windows the predicted stress is 1,400 psi, much less than the tensile strength of the quartz, even when safety factors are taken into account.

No failure at this thickness would be expected, and none of the $\frac{1}{2}$ " windows employed have failed.

APPENDIX B

DERIVATION OF EQUALITY OF PHASE VOLUMES AT CRITICAL POINT

The volumes of the sample cell and of the liquid and the gas phases below the critical temperature are given by V , V_L , and V_G , with $V = V_L + V_G$. ρ is the average number density in the sample cell, with the number density of the gas and the liquid phases given by ρ_G and ρ_L . The total number of molecules present is given by N , with $N = \rho V$. Similar equations describe the number of molecules present in each of the two phases:

$$N_L = \rho_L V_L; \quad N_G = \rho_G V_G$$

The total number of molecules present is the sum of the number of molecules in each phase

$$N = N_L + N_G$$

which may be written

$$\begin{aligned} N &= \rho_L V_L + \rho_G V_G \\ &= \rho_L V_L + \rho_G (V - V_L) \end{aligned}$$

The volume of the liquid phase may be calculated in terms of these quantities

$$\begin{aligned}
 V_L &= \frac{N}{(\rho_L - \rho_G)} - \frac{V \rho_G}{(\rho_L - \rho_G)} = \frac{N - V \rho_G}{(\rho_L - \rho_G)} \\
 &= \frac{V(\rho - \rho_G)}{(\rho_L - \rho_G)}
 \end{aligned}$$

with the relative volume given by

$$\frac{V_L}{V} = \frac{\rho - \rho_G}{\rho_L - \rho_G}$$

According to the definition of the order parameter

$$(\rho_L - \rho_C) = (\rho_C - \rho_G) = B \epsilon^\beta$$

close to its critical point. Then

$$\rho_G = \rho_C - B \epsilon^\beta$$

$$\rho_L = \rho_C + B \epsilon^\beta$$

with

$$\rho_L - \rho_G = 2B \epsilon^\beta$$

the relative volume then becomes

$$\frac{V_L}{V} = \frac{\rho - \rho_C + B \epsilon^\beta}{2B \epsilon^\beta} = \frac{\rho - \rho_C}{2B \epsilon^\beta} + \frac{B \epsilon^\beta}{2B \epsilon^\beta} = \frac{\rho - \rho_C}{2B \epsilon^\beta} + \frac{1}{2}$$

which reduces to

$$V_L = \frac{1}{2}$$

when $\rho = \rho_c$. The volumes of the two phases are then equal to the critical point when the average density inside the cell is equal at the critical density.

APPENDIX C

Computer Program LSQG for Generalized Least Squares Fit

```

PARAMETER ML=200,MM=10
DIMENSION IX(MM),XX(MM),X(ML,MM),Y(ME),Z(ME),FF(MM,MM),F(MM),C(ME)
DATA Z/NE*1./
NAMelist/RO/NE,C,IX,X,Y,Z,LX
100 FORMAT(// ' 3RD C,NE,IX,X,Y,Z,LX')
101 FORMAT(// ' I)ADEQUATE DATA ')
102 FORMAT(//1X,'CHI**2/N=',G11.4//7X,'I',8X,'PAR',8X,'ERR'/
C (I8,3Y,2G11.4))
103 FORMAT(// ' INPUT DATA ')
104 FORMAT(I8,3X,(5G11.4))
CALL BPKY(51)
1 WRITE(6,100)
HEAD(5,RO,ERR=1,END=99)
DO 3 I=1,MM
IF(IX(I).EQ.0) GO TO 3
DO 2 IF=3,NL
2 X(IE,I)=2.*X(IE-1,I)-X(IE-2,I)
3 IX(I)=0
DO 4 I=1,MM
DO 4 I1=1,MM
4 FF(I,I1)=0.
GG=0.
NH=0
DO 8 IF=1,NE
DO 5 I=1,MM
5 XX(I)=X(IE,I)
CALL FMS(C,XX,Y(IE),Z(IE),NF,F,G,H)
IF(H.LF.0.) GO TO 8
NI=NF+1
DO 7 I=1,NF
DO 6 I1=1,NF
6 FF(I,I1)=FF(I,I1)+H*F(I)*F(I1)
7 FF(I,NI)=FF(I,NI)+H*F(I)*G
GG=GG+H*G**2
8 NH=NH+1
DO 9 I=1,NI
DO 9 I1=1,I
9 FF(I,I1)=FF(I1,I)
K=1
CALL INVM(MM,NF,FF,K,D)
IF(K.EQ.0) GO TO 10
WRITE(6,101)
GO TO 13
10 DO 11 J=1,NF
11 GG=GG-FF(NI,I)*FF(I,NI)
GG=GG/NH
DO 12 J=1,NF
12 FF(NI,I)=SORT(ABS(FF(I,I)*GG))
WRITE(6,102)GG,(I,FF(I,NI),FF(NI,I)),I=1,NF)
13 IF(LX.FW.0) GO TO 1
WRITE(6,103)
DO 14 IL=1,NE
14 WRITE(6,104)IL,(X(IL,I),I=1,LX),Y(IE),Z(IF)
GO TO 1
99 END

```

END ONSITE PRINTOUT ON DECEMBER 18, 1973 AT 21:17:44

BIBLIOGRAPHY

1. T. Andrews, Phil. Trans. Roy. Soc. (London) 159, 575 (1869)
2. J. D. van der Waals, PhD thesis, On the Continuity of the Gaseous and the Liquid State (1873)
3. M. von Smoluchowski, Ann. Physik 25, 205 (1908)
4. A. Einstein, Ann. Physik 33, 1275 (1910)
5. L. S. Ornstein, F. Zernike, Proc. Akad. Sci. 17, 793 (1914) Reprinted in The Equilibrium Theory of Classical Fluids, ed by H. L. Frisch and J. E. Lebowitz (1964)
6. F. J. Schoenes, Ber. Bun. Ges. 76, 228 (1972)
7. J. A. White and B. S. Maccabe, Phys. Rev. Letters 26, 1468 (1971)
8. A. V. Voronel et al, Sov. Phys.-JETP 18, 568 (1964)
9. A. Michels, J. Strijland, Physica 18, 613 (1952)
10. M. E. Fisher, J. Math. Phys. 5, 944 (1964)
11. H. E. Stanley, Introduction to Phase Transitions and Critical Phenomena (International Series of Monographs on Physics) (1971)
12. J. E. Thomas, P. W. Schmidt, J. Chem. Phys. 39, 2506 (1963)
13. W. P. Kao, B. Chu, J. Chem. Phys. 50, 3986 (1969)
14. A. Michels, B. Blaisse, C. Michels, Proc. Roy. Soc. (London) A160, 358 (1937)
15. E. A. Guggenheim, J. Chem Phys. 13, 253 (1945)
16. L. P. Kadanoff et al, Rev. Mod. Phys. 39, 395 (1967)
17. J. M. H. Levelt Sengers, J. Straub, and M. Vicentini-Missoni, J. Chem. Phys. 54, 5035 (1971)
18. P. Heller and G. B. Benedek, Phys. Rev. Letters 14, 71 (1965)
19. J. A. Lipa, C. Edwards, and M. J. Buckingham, Phys. Rev. Letters 25, 1086 (1970)

20. J. H. Lunacek and D. S. Cannell, Phys. Rev. Letters 27, 841 (1971)
21. C. J. Pings, paper presented at the Van der Waals Centennial Conference on Statistical Mechanics (1973) to be published in Physica
22. P. R. Roach, Phys. Rev. 170, 313 (1968)
23. J. M. H. Levelt Sengers, paper presented at the Van der Waals Centennial Conference on Statistical Mechanics (1973) to be published in Physica
24. H. W. Habgood and W. G. Schneider, Can. J. Chem. 32, 98 (1954)
25. C. Edwards, J. A. Lipa, and M. J. Buckingham, Phys. Rev. Letters 20, 496 (1968)
26. M. Kac, G. E. Uhlenbeck, P. E. Hemmer, J. Math Phys. 4, 216 (1963)
27. L. Onsager, Phys. Rev. 65, 117 (1944)
28. R. B. Griffiths, Phys. Rev. Letters 14, 623 (1965)
29. G. S. Rushbrook, J. Chem. Phys. 39, 842 (1963)
30. M. E. Fisher, lecture presented at the Theoretical Physics Institute, University of Colorado, Summer 1964, reprinted in Lectures in Theoretical Physics, ed by W. E. Brittin (1965)
31. B. Widom, J. Chem. Phys. 37, 2703 (1962)
32. M. E. Fisher, Rpts. Prog. Phys. 30, 615 (1967)
33. J. A. Gonzalo, Phys. Rev. 144, 662 (1966)
34. G. B. Benedek, Thermal Fluctuations and the Scattering of Light, from Brandeis University Summer Institute in Theoretical Physics, 1966
35. H. L. Swinney and H. Z. Cummins, Phys. Rev. 171, 152 (1968)
36. J. D. Jackson, Classical Electrodynamics p. 109 (1962)
37. M. Kerker, The Scattering of Light and other Electromagnetic Radiation p. 38, Academic Press, New York (1969)
38. Critical Phenomena, N. B. S. Misc. Publ. No. 273, Eds. M. S. Green and J. V. Sengers (Washington: National Bureau of Standards), 1966
39. Handbook of Chemistry and Physics, 49th edition, Ed. by R. C. Weast,

- Chemical Rubber Company, Cleveland, Ohio (1968)
40. G. W. Morey, J. Am. Chem. Soc. 36, 215 (1914)
 41. Handbook of Engineering Fundamentals, 2nd Edition, Ed. by O. W. Eshbach, J. Wiley and Sons, New York (1936)
 42. Matheson Gas Data Book by W. Bracker and A. L. Mossman, East Rutherford, New Jersey (1971)
 43. International Critical Tables, McGraw-Hill Book Co., New York (1928)
 44. P. Villard, Compt. Rend. 118, 1096 (1894)
 45. D. Kuenan, Phil. Mag. 40, 173 (1895)
 46. E. Cardoso and E. Arni, J. Chim. Physique 10, 505 (1912)
 47. E. L. Quinn and G. Wernimont, J. Am. Chem Soc. 51, 2002 (1929)
 48. D. Cook, Trans. Faraday Soc. 49, 716 (1953)
 49. L. F. Albright and J. J. Martin, Ind. Eng. Chem. 44, 188 (1952)
 50. J. Collie, J. Chem. Soc. 55, 110 (1889)
 51. Fenwal Electronics Inc. Data Sheet, Framingham, Massachusetts
 52. D. R. Corson and P. Lorrain, Introduction to Electromagnetic Fields and Waves, W. H. Freeman and Co., San Francisco (1962)
 53. V. G. Puglielli and N. C. Ford, Phys. Rev. Letters 25, 143 (1970)
 54. Data Sheet for GE 125 Fused Quartz, Bond Optics, Div. Bond Research Labs, Lebanon, N. H.

VITA

Edward Patterson was born December 11, 1943 in Savannah, Georgia. He attended Benedictine Military School and graduated in 1961. After entering the Georgia Institute of Technology as a freshman, he received a Bachelor of Science in Physics in 1965, and a Master of Science in Physics in 1967 from the same institution.

While a graduate student at the Georgia Institute of Technology Mr. Patterson worked as a laboratory and teaching assistant. In the summer of 1967 he was awarded a National Science Foundation Traineeship. He was employed by Clark College from 1970 to 1973 as an instructor in the Cooperative General Science Program.

He was married to Marjorie Dees of Jasper, Florida, in December, 1971.